Manuscript Details

Manuscript number	MTENER_2017_267
Title	All Nanocarbon Li-Ion Capacitor with High Energy and High Power Density
Article type	Research Paper

Abstract

An energy storage device reaching energy densities of 102 Wh/Kg at power densities of 104 W/Kg would mean the possibility of charging such a device in 36 seconds. The nanocarbon device presented here is closer to that feat than any previously reported system. N-doped Carbon Nanopipes were used as negative electrode and Partially Reduced Graphene Oxide (PRGO) as positive electrode, with LiPF6 EC/PC electrolyte. This system yields simultaneously high energy and power densities (262 at 450 W/kg and 78 Wh/kg at 9000 W/kg) which are energy/power combinations significantly higher than those of present LIBs. Our cell exhibits excellent cycle stability (□91 % capacity retention after 4000 cycles 0.01 to 4 V). These breakthrough results are based on the kinetic balancing of the nanocarbon electrodes, which can deliver the holy grail of energy storage, namely, by providing high energy density at high rates and low costs.

Keywords	Nanocarbon; Li-ion capacitor; High energy density
Corresponding Author	Deepak Dubal
Corresponding Author's Institution	Catalan Institute of Nanoscience and Nanotechnology, CIN2, ICN2 (CSIC-ICN)
Order of Authors	Deepak Dubal, Pedro Gomez-Romero
Suggested reviewers	Rongming Wang, Keryn Lian, Y.P. Wu

Submission Files Included in this PDF

File Name [File Type]

Response Letter.docx [Cover Letter]

Final Manuscript_ASS.doc [Manuscript File]

To view all the submission files, including those not included in the PDF, click on the manuscript title on your EVISE Homepage, then click 'Download zip file'.

To,

The Editor,

Materials Today Energy

Subject: *Resubmission of Article reference number: JOULE-D-17-00140 suggested by the Editor of Joule.*

Dear Editor,

Herewith, we are resubmitting a revised version of our investigation entitled ***"All Nanocarbon Li-Ion Capacitor with High Energy and High Power Density"*** *Deepak P. Dubal,* Pedro Gomez-Romero** for publication in ***Materials Today Energy*.**

We sincerely appreciate the editor and reviewers for reviewing and suggesting valuable comments to improve our manuscript. Following your request letter on 4 September 2017 (from Joule), we have thoroughly revised our manuscript to accommodate all the comments and issues raised by the editor and reviewers. We have made substantial modifications to address the reviewer's suggestions and comments as well as other changes that we thought appropriate to improve our manuscript. Point by point response to reviewer's comments are described in detail from following page. We would like this revised version to be reconsidered with the reviewers' further evaluations and sincerely hope that our revised manuscript satisfies you and the reviewers for publication to the ***Materials Today Energy***.

Please feel free to contact us for any further information.

Thank You

***Dr. Deepak P. Dubal*,**

UoA Vice Chancellors Fellow,

Former Marie-Curie and Alexander von Humboldt Fellow

School of Chemical Engineering,

The University of Adelaide,

Adelaide, SA 5005, Australia

Reviewer #1:

1. For PRGO cathode, it shows a maximum capacity of 171 mAh/g (~205 F/g) at 0.17 A/g, which is considerably higher than that of activated carbon or other carbon-based cathodes? The specific capacity is very large, why does this phenomenon happened? The detailed energy storage mechanism should be given. "RSC Adv., 2013, 3: 20024-20033", may give some reference.

Answer: Thank you for the comment. The reference is cited in the revised version of manuscript.

2. For PRGO, the O content is 34.9 %, that value is very large. What about the O content of GO. If there are too much O, the electronic conductivity should be lower, please give more information about the electronic conductivity of PRGO. "Advanced Energy Materials, 2016, 6: 1600426", "Nanoscale, 2015, 7: 8819-8828" may give some reference.

Answer: We appreciate reviewer's comment on the electronic conductivity of GO. In present paper, we have intentionally maintained the large amount of O functional groups so that we can take advantage of pseudo-capacitance between Li-ions and O-groups and achieve enhanced electrochemical performance. According to reviewer's comment, we have included explanation and cited mentioned references in the text.

3. When calculated the Ragone plot of the N-CNPipes//PRGO LIC cell, which weight was chosen, the weight of active materials or the cell? If only the weight of active material was chosen, it should be divide by 3 or 4 for practical cell. "Energy & Environmental Science, 2015, 8: 869-875" may give some reference.

Answer: We appreciate reviewer's comment. However, all the calculations have been carried out using weight of active materials, which is already mentioned in the manuscript. In addition, the values are compared with the values calculated using weight of active materials in the Ragone plot. The values for devices has been mentioned in the text by dividing 4 for practical cell.

4. It also have some mistake need the author to double check. For example: "At scan rate of 1 mV/s, the capacitive and diffusion charge contributions are 56.4 % and 44.8 %, respectively, while at high scan rate of 10 mV/s, the capacitive charge is 93.1 % due to the faster charge kinetics."

Answer: The manuscript is thoroughly revised and modified accordingly.

Reviewer #2:

The material used for the anode is termed carbon nanopipes - and could just as easily been called multi-wall carbon nanotubes. The authors characterize the structure and chemistry of their material but do not really distinguish it from carbon nanotubes. The high lithium capacity they report for this material, ~ three times greater than graphite, is something that has also been reported for other carbon systems. In most cases, the reason for the higher capacity (at slow rates) has to do with slight dissolution of the lithium counter electrode in the electrolyte. Thus, the high levels of energy storage arise primarily from the plating and stripping of the SEI and not from intercalation or other mechanisms. The proper experiment to run in this case is to use an overcapacitive carbon counter electrode in both galvanostatic and potentiostatic measurements. It is strongly recommended that the authors carry out these experiments before they make speculative claims that this extraordinary capacity is from the graphitic and pyridinic nitrogens in their material.

Answer: We partially appreciated with the reviewer's comment. The carbon nanopies and multi-walled carbon nanotubes are totally different, which we have proved with many characterizations such as XRD, Raman and HRTEM images. It is clearly evidenced that the inner diameter of the CNTs is very close to 15 to 20 nm however CNPipes exhibits inner diameter in the range of 45 to 60 nm with very thin walls. Another important difference between CNPipes and MWCNTs is their graphitic structure. The CNPipes exhibited distorted graphitic structure with graphitic and pyridinic nitrogen doping as compared to MWCNTs. We agree with reviewer's comment that the high lithium capacity achieved due to the plating and stripping of the SEI. However, we cannot ignore the possibility of intercalation mechanism, which is evidenced from the HRTEM images provided in supporting information S. I. S6.

Another inappropriate explanation has to do with the authors asserting that the high capacity for the partially reduced graphene oxide (PRGO) comes from redox reactions with oxygen functional groups on the surface. First, the authors provide no evidence of any redox reactions with the carbon groups. Moreover, the supercapacitor community has shown through experiments and simulations that the broad 'peaks' in the CV are not from redox reactions but instead arise from a decrease in ion adsorption at high voltage. The authors are encouraged to carry out well designed charge transfer reactions in order to prove that the peaks are from redox reactions.

Answer: Reviewer misunderstood with the word "redox reactions". The term is basically used to represent "pseudo-capacitive" mechanism, which is surface redox reactions. We are aware of

capacitive (rectangular), pseudo-capacitive (rectangular) and faradic (redox peaks) mechanisms. In present paper, we have not claimed that the peaks corresponds to faradic reactions.

As for the LIC devices, the authors have not solved the key technological problem of providing an in-situ or internal source of lithium. Instead the authors used the same approach as others, namely disassembling a lithiated half-cell and using that as the electrode. The energy and power densities reported here are good but one must recognize that the authors are operating a 4V cell. Most of the comparisons they make are with systems that have a lower voltage and, correspondingly, lower energy density.

Answer: In this investigation, we have proposed a novel combination such as N-CNPipes//PRGO hybrid system. The technological problem can be easily solved by coating stabilized lithium metal powder (SLMP) on the electrode surface, which can be used as internal source of lithium [1]. We are not agree with reviewer's comment that we have only compared energy and power densities with low voltage cells. In Table 2 (supporting information), we have compared electrochemical performances of the Li-ion capacitors, which have large voltage windows up to 4.5 V.

[1] Z. Wang, Y. Fu, Z. Zhang, S. Yuan, K. Amine, V. Battaglia, G. Liu, J. Power Sources, 260, 57-61 (2014)

All Nanocarbon Li-Ion Capacitor with High Energy and High Power Density

Deepak P. Dubal,[a, b] Pedro Gomez-Romero [a]**

[a]Dr. Deepak P. Dubal, Prof. Pedro Gomez-Romero

[a]Catalan Institute of Nanoscience and Nanotechnology (ICN2), and The Barcelona Institute of Science and Technology (CSIC-BIST), Campus UAB, Bellaterra, 08193 Barcelona, Spain

E-mail: dubaldeepak2@gmail.com (D. Dubal),pedro.gomez@icn2.cat (P. Gomez-Romero)

[b]Dr. *Deepak P. Dubal*

School of Chemical Engineering, The University of Adelaide, Adelaide, South Australia 5005, Australia

Keywords: All Nanocarbon, Li-ion capacitor, High energy density

Abstract

An energy storage device reaching energy densities of 10^2 Wh/Kg at power densities of 10^4 W/Kg would mean the possibility of charging such a device in 36 seconds. The nanocarbon device presented here is closer to that feat than any previously reported system. N-doped Carbon Nanopipes were used as negative electrode and Partially Reduced Graphene Oxide (PRGO) as positive electrode, with $LiPF_6$ EC/PC electrolyte. This system yields simultaneously high energy and power densities (262 at 450 W/kg and 78 Wh/kg at 9000 W/kg) which are energy/power combinations significantly higher than those of present LIBs. Our cell exhibits excellent cycle stability (~91 % capacity retention after 4000 cycles 0.01 to 4 V). These breakthrough results are based on the kinetic balancing of the nanocarbon electrodes, which can deliver the holy grail of energy storage, namely, by providing high energy density at high rates and low costs.

Introduction

In the world of energy storage, supercapacitors and batteries constitute the most obvious example that you can't have it all. Or can you? High-power-density supercapacitors (SCs) are handicapped by low energy densities whereas the best among batteries, Li-ion batteries (LIBs), feature the best energy densities but lag behind in power. Yet, they both are in the midst of intense developments given the expansion of energy storage markets [1, 2]. These complementary drawbacks hamper the applications of SCs and LIBs when both high energy and high power densities are essential. Thus, the race is on to develop new energy storage materials and systems which could deliver high energy at high rates. [3-5] And, of course, at low cost.

On the other hand, the complementarity of supercapacitors and batteries allows for a positive view of the question by considering the development of hybrid devices, electrodes or materials which could combine the faradaic processes of batteries with the capacitive mechanism of supercapacitors in a synergic combination [6, 7]. Lithium Ion Capacitors (LICs) are precisely that; hybrid arrangement of a battery-like electrode (as a negative) and supercapacitor-like electrode (as a positive) in organic electrolyte, [6-9] heading to enhanced energy and power densities [10]. Moreover, LICs don't suffer the substantial volume changes and phase transitions of battery electrodes, thus featuring excellent cycle life, comparable to that of SCs.

On the other hand, all the recent progress in LICs has not solved a serious intrinsic drawback, namely, the imbalance of kinetics between the two electrodes. Indeed, the fast double layer polarization in the capacitive electrode is handicapped by the much slower electro-ionic process of the battery electrode. Thus, the greatest challenge in order to assemble truly high-performance LICs is to pair suitable capacitor-type and battery-type electrodes in a kinetically balanced device. One obvious but difficult way to do this is to use fast surface reactions in both cathode and anode without sacrificing energy density [11-13].

Recently, Kang and co-workers [14, 15] showed that the partial reduction of graphene oxide allows for swift surface reactions with substantial enhancement of Li storage capacity due to the existence of oxygen functional groups. Furthermore, it is also well established that heteroatom doping (such as N for C) in the graphitic layers of carbon materials is an efficient strategy to modify their basic [16, 17] and electrochemical properties as anode materials [18, 19].

Here we report our design and demonstration of an innovative LIC cell by coupling rapid surface reactions from two distinct nanocarbon electrodes, namely, a cathode made of partially reduced graphene oxide (PRGO) and an anode of nitrogen-doped open-end ultralong carbon nanopipes (N-CNPipes). We expected this novel type of LICs to be able to deliver remarkably high power densities due to a unique combination of features, namely, i) swift surface reactions of both positive and negative electrodes, ii) unique interconnected nanosheets-like porous nanostructure, iii) good electrical conductivity and iv) defects in graphitic walls of N-CNPipes allowing for effective diffusion of Li^+ . These unique characteristics of PRGO cathode and N-CNPipes anode have led to a hybrid cell combining the best characteristics of LIBs and supercapacitors to fill the performance gap between them thanks to a kinetically balanced electrode pair. Finally, it should be emphasized that both of these nanocarbon materials can be easily produced at large-scale and hence, eventually, at low costs.

Results and Discussion

Fabrication of N-CNPipes anode and half-cell characterizations

Ultra-long open-end nitrogen-doped carbon nanopipes (N-CNPipes) were prepared by pyrolysis of conformal polypyrrole nanopipes (PPy-NPipes) at 800 °C under N_2 atmosphere (see supporting information S. I. S1). The detailed growth mechanism of hollow polypyrrole nanopipes (PPy-NPipes) is explained elsewhere [20, 21]. XRD pattern of N-CNTs shows a weak peak at around 25.5º which is characteristic of carbon based materials (see S. I. 2). The amorphous nature further confirms the formation of disordered carbon structure which can be beneficial for energy storage applications due to the easy transportation of ions (from electrolyte). The amount of nitrogen and its bonding environment in N-CNPipes was investigated by XPS analysis. Full XPS spectrum of N-CNPipes shows main peaks centered at 284.3 eV (C1s), 400.1 eV (N1s), and 533.2 eV (O1s), respectively (see S.I. S3). The C1s spectrum (Figure 1 a) was fitted with three peaks at binding energies of 284.6, 285.5 and 287.7 eV corresponding to pyrolytic graphite of sp^2 C=C, C-O and C-N species, respectively [22]. Furthermore, the magnified view of N1s exhibits two distinct peaks centered at 398.2 eV and 400.7 eV as shown in Figure 1 (b).

During the preparation of N-CNPipes at 800 °C, nitrogen atoms from polypyrrole integrate into the graphene layers. The XPS peaks observed in the ranges of 398-399 and 400-401.5 eV are assigned to pyridinic N (bonded to two sp^2 carbons) and graphitic N (bonded to three sp^2 carbons) respectively [23, 24]. The amount of nitrogen in N-CNPipes was calculated by the ratio of the area of the N peak and the sum of C and N peaks (N/(C + N)), and was found to be a remarkable 12.5 atom %, significantly larger than earlier reports on similar materials [16, 25].

The Raman spectrum shows two characteristic peaks at 1355 (D band) and 1571 cm^{-1} (G band) which are assigned to lattice defects and to pyrolytic graphite respectively (S. I. 4).

The I_G/I_D ratio of 0.96 for N-CNPipes indicates the formation of nanopipes with extra defects and active sites due to nitrogen doping.

Figure 1 (c) shows a FESEM image of N-CNPipes with a great number of ultralong nanopipes (average length of a few microns) with smooth surfaces and transparent enough to confirm their hollow nature (S.I. S3). At low magnification, the TEM image reveals the formation of ultralong nanopipes several micrometers in lengths while the high magnification TEM image confirms the open ends of N-CNPipes (S.I. S4). The nanopipes have inner and outer diameters in the range of 45-50 and 70-80 nm, respectively with relatively thin walls of 17-19 nm (Figure 1 (d)). These large diameters prompted us to label them nanopipes instead of nanotubes, in order to remark the difference with conventional single or multiwalled CNTs, a difference which has great implications in the performance of these new nanocarbon materials for energy storage.

A limited extent of graphitization is observed in HRTEM (Figure 1 e), confirming the formation of structural defects due to N doping. In order to get information about the distribution of nitrogen in these CNPipes, EFTEM with EDS mapping analysis were performed and displayed in Figure 1 (f). It is clearly seen that the nitrogen is uniformly distributed over the whole carbon nanopipes surfaces. The BET surface area and pore-size distributions measurements of N-CNPipes were further carried out and shown in S.I. S2. The specific surface area was found to be 77 m^2/g and exhibits most of the pores in mesoporous regime with central maximum at 4 nm. These mesopores can provide “super highways” for the electrolyte ions within the porous network and shorten the diffusion length.

The electrochemical properties of N-CNPipes as anode material for LIBs were investigated in Li-ion half-cells as shown in Figure 2. The N-CNPipes electrode exhibits a cyclic voltammogram (CV) (Figure 2 (a)) typical of carbon-based anode materials [26], suggesting lithiation (charge) and delithiation (discharge) reactions. During, the first cathodic scan, an obvious broad peak at ~0.5 V is observed which corresponds to the solid-electrolyte-interphase (SEI) layer formed due to the decomposition of electrolyte. This peak is absent in subsequent

cycles indicating that the SEI layer is significantly stable, which further decreases the irreversible capacity. Figure 2 (b) shows the charge/discharge curves of N-CNPipes for the first four cycles at 0.1 A/g current density. Initially, the voltage drops quickly and creates a plateau at 0.9-0.7 V during the first cycle, which is attributed to the SEI layer [25], in agreement with the CV results. The initial reversible capacity was found to be 982 mAh/g which is almost three times higher as compared to the graphite's theoretical capacity (372 mAh/g). The lithium storage mechanism in N-CNPipes is still not clear (as it is also the case for conventional CNTs). However, it is presumed that lithium ions can diffuse into the disorder graphitic carbon layers and interact with N functional groups, heteroatoms and defects [27]. In order to provide deeper insights, used N-CNPipes electrode was characterized after 1000 charge/discharge cycles (S.I. S5). The XRD and XPS analyses provide evidence for the expected formation of an SEI layer, confirmed for example by the presence of Li_2CO_3. On the other hand, the absence of characteristic peaks of the LiC_6 phase, which is the typical intercalated state [28] in graphite anodes, suggests other alternative Li insertion mechanism. Recent reports [29-31] suggest that a high reversible specific capacity of graphene could be associated to lithium plating/deposition within the defective porous graphene. In our investigation, the XPS Li1s spectrum could be fitted with two peaks of binding energies 55.6 and 56.1 eV, respectively (S.I. S5) which can be assigned to the binding of Li to N (Li-N) and LiF, respectively [32, 33]. On the other hand, it is very important to note that SEM and TEM images do not show any signs of dendritic or metallic lithium growth, suggesting the formation of a novel Li-carbon material which effectively confines Li inside the graphitic carbon layers and prevents the growth of dendrites. HRTEM images further suggest the improved size of the N-CNPipes, in particular the wall thickness suggesting an interwall Li-storage mechanism (S. I. S6). At the same time, during the first cycle, a large irreversible capacity of 1992 mAh/g is obtained, associated to the SEI layer at the N-CNPipes electrode which is common to all carbon anodes. However, in this particular case, extremely stable and reversible capacity of 982 mAh/g is achieved after the first cycle which is the

considerably higher than the values reported so far for carbon based anode materials (See S.I. Table 1). The super-high reversible capacity may be attributed to the graphitic and pyridinic nitrogens which create defects in N-CNPipes and could favor Li reduction.

A high rate capability is another key factor for the success of LIBs in many applications such as HEVs where rapid discharge/charge rates are required [34, 35]. The rate capability of N-CNPipes anode at different current densities from 0.1 A/g to 20 A/g was investigated (S. I. S7). Notably, the N-CNPipes show excellent Li-ion storing capability and cycling stability even at high rates. The reversible capacities are 982 and 166 mAh/g at 0.1 and 20 A/g, respectively (Figure 2 c). It should be underscored that the N-CNPipes show a reversible capacity of 166 mAh/g even at the very high current density of 20 A/g, which is still a very substantial value (around 50 % of graphite's theoretical capacity). Moreover, after changing the current density to 0.1 A/g after 100 cycles at various current densities, the N-CNPipes achieve a capacity of 972 mAh/g, suggesting excellent rate capability. The cycling performance of N-CNPipes was investigated at 0.5 A/g over 1000 cycles and is displayed in Figure 2 (d). They present an extraordinary cycling stability during charge/discharge with a final capacity of 355 mAh/g after 1000 cycles which is considerably better than the theoretical capacity of graphite. Thus, the N-CNPipes exhibit exceptionally good Li-ion storage performance when compared with other carbon-based anode materials previously reported (S.I. Table 1) [26, 36, 37]. Finally, although the coulombic efficiency of N-CNPipes electrodes was initially low (54.7 %) it increased with cycling and finally reached values greater than 90% in the next 10 cycles, stayed at 98 % for 300 cycles and slightly decreased to 95.2 % until completion of the first 1000 cycles. This exceptional long-term stability may be ascribed at least in part to the hollow nanopipes buffering a volume expansion during charging/discharging.

In order to further understand this excellent Li-ion charge kinetics, the capacitive and diffusion contributions to the total charge stored in N-CNPipes were estimated by the methods reported elsewhere [38]. Figure 3 (a) shows the schematic representation of possible charge

storing mechanism in N-CNPipes. For this analysis, the CV curves for N-CNpipes were recorded at different scan rates (S. I. S7). The slope of the corresponding log(ν) vs log(i) plot in Figure 3 (b) is b = *0.89* for anodic peak and is consistent with kinetics dominated by surface capacitive-controlled process. Thus, the total current response of the electrode as measured with CV is the sum of surface capacitive charge (Q_c) and diffusion-controlled charge (Q_d and can be expressed as follows,

$$Q_t = Q_c + Q_d \quad (1)$$

The capacitive contribution (Q_c) is associated with the charges stored at the electrode/electrolyte interface and hence are scan rate independent. Moreover, Q_c is assumed to be the combination of both pseudocapacitance (surface redox reactions) and electrical double layer capacitance (see Figure 3a). Semi-infinite linear diffusion is assumed for the diffusion processes of Q_d, and thus, Q_d varies as the reciprocal square root of scan rate. Thus, the equation (1) for the total charge contribution (Q_t) can be rewritten as follows,

$$Q_t = Q_c + k\nu^{-1/2} \quad (2)$$

Where, k is a constant and Q_c can be determined by plotting Q_t against the reciprocal of the square root of scan rate ($\nu^{-1/2}$). Figure 3 (c) presents the capacitive and diffusion controlled charge contribution at different scan rates. The charge contribution analysis suggests that both capacitive and diffusion charges contributes nearly equal to the total charge stored in the N-CNPipes. At scan rate of 1 mV/s, the capacitive and diffusion charge contributions are 56.4 % and 44.8 %, respectively and at a high scan rate of 10 mV/s, the capacitive contribution 93.1 %. A significant capacitive charge contribution is attributed to the pseudocapacitance arising due to the surface redox reactions between Li-ions and N-functional groups on the surface of N-CNPipes [39]. In addition, the defects induced on the graphene layers create a disordered carbon structure (see Figure 3 a) which further advances the Li-ion adsorption properties [40].

On the other hand, the Li-ion can also accommodate in the graphene layers which additionally contributes to store the extra Li-ions in the N-CNPipes.

The Li-ion diffusion coefficient in N-CNPipes electrode was further estimated by the Randles-Sevick equation [41]:

$$i_p = 2.69 \times 10^5 n^{3/2} A D_{Li}^{1/2} \nu^{1/2} C \quad (3)$$

where i_p is current maximum in amps (we considered current value at 3 points), n is number of electrons involved in the charge storage, A is electrode area in cm^2 (for simplicity we have considered geometrical area), D_{Li} is diffusion coefficient in cm^2/s, ν is scan rate in V/s, C is concentration of Li-ion in mol/cm^3. The diffusion coefficients for N-CNPipes are in the range of 10^{-10} cm^2/s for different scan rates (Figure 3d) which are comparable or slightly greater than the values reported for carbon-based materials [42-44]. The diffusion coefficients for N-CNPipes slightly changes with increasing scan rate (the order 10^{-10} remains same), further confirming the high rate capability of the material. Obviously, the capability for diffusion of lithium ions in N-CNPipes is better than the previously reported carbon materials and this advantage will expand remarkably with increase of lithium ion contents, which results in a great improvement of rate performance. This high diffusion coefficient may be attributed to the unique nanopipes-like nanostructure where the Li^+ ions can enter into the pipes and can diffuse into the defect induced graphene layers from both the external and inner surfaces (Figure 3 a). Due to all these reasons, N-CNPipes presented in this investigation shows excellent Li-ion performance as compared to the other carbon materials as well as conventional nanotubes.

Fabrication of PRGO cathode and half-cell characterizations

Graphene, the two-dimensional wonder material, has boomed in the field of energy storage and conversion in a very short time [45]. We have used partially reduced graphene oxide (PRGO) cathodes as the positive electrode counterpart to N-CNPipes anodes.

First of all, graphene oxide (GO) was prepared by a modified Hummers method as described in the experimental section. In order to prepare partially reduced GO (PRGO), graphene oxide was annealed at 120 °C for 6 h. The characteristic XRD peak observed at 26° for graphite is shifted to a lower angle after partial reduction of GO due to an expansion of the interlayer spacing in graphene oxide (S.I. S8). Moreover, XRD peaks get broader and weaker after partial reduction, due to the loss of long-range order. Furthermore, XPS showed the presence of carbon (286 eV) and oxygen (530 eV) as shown in S.I. S8, which confirms the introduction of oxygen functional groups on GO nanosheets. The oxygen content was found to be around 34.9 % confirming the formation of partially reduced graphene oxide (PRGO). The C1s spectrum was fitted with three peaks centered at 284.6, 286.2 and 287.7 eV, corresponding to C-C, C-O and C=O, respectively, further confirming the presence of considerable amounts of oxygen (S.I. S8). Furthermore, the O1s peak could be fitted so that the peak entails primarily carbonyl groups (C=O) at 531.5 eV, and C-O at 533.4 eV as seen from S.I. S8.

In addition to proper functional groups an optimal electrode material must have a porous microstructure for high electrochemical performance, since open-porosity enables greater permeation of the electrolyte ions into the bulk of the electroactive materials. Figure 4 (a) shows FESEM and TEM (inset of Figure 4a) images of PRGO cathode. Remarkably, PRGO exhibits three dimensional (3D) networks of open-porous interconnected nanosheets (see S.I. S9). The formation of open-porosity in PRGO is attributed to the fast gas release under the high vapor pressure produced due to the concentrated HCl treatment [14].

The electrochemical performance of the PRGO cathode was initially measured in a Li half-cell system between 1.5-4.5 V vs. Li/Li^+ and is displayed in Figure 4 (b-c). The CV curves of PRGO reveal nearly rectangular shapes with small humps observed at all the scan rates measured, indicating major contribution from EDLC with a smaller but considerable share from pseudo-capacitance (S.I. S10). This pseudo-capacitance must be ascribed to the presence of oxygen functional groups on PRGO nanosheets. Figure 4 (b) shows galvanostatic charge-

discharge (GCD) curves of PRGO at different current densities from 0.17 A/g to 8.71 A/g. The linear and symmetric nature of these GCD profiles further confirms the capacitive behavior of this electrode material through adsorption/desorption of PF_6^- anions. Impressively, the PRGO cathode shows a maximum capacity of 171 mAh/g (~205 F/g) at 0.17 A/g which is considerably higher than that of activated carbon or other carbon-based cathodes [46-49]. Moreover, the PRGO cathode still delivers a capacity of 92.3 mAh/g at very high current density of 8.71 A/g, suggesting excellent rate capabilities (see Figure 4 c). This excellent performance of PRGO might be attributed to the partial reduction of graphene oxide which increases electrical conductivity while maintaining a substantial amount of C=O redox groups. The cycling test reveals that after 5000 cycles at 0.34 A/g the PRGO electrode retains 93 % of its initial specific capacity, with a Coulombic efficiency of 100 % as shown in Figure 4 (d).

PRGO cathodes show high charge storage capabilities thanks in part to their pseudocapacitive mechanism, involving redox reactions of functional groups (C=O/C–O) with the consequent Li+ uptake. On the other hand, this pseudo-capacitive component has no detrimental effect on cycling because the reactions involved are molecular redox processes and do not involve phase transitions or volume change during charge/discharge (see S.I. S11).

Considering all these excellent electrochemical properties of PRGO in $LiPF_6$ electrolyte and its complementary electrochemical voltage, PRGO was anticipated to be a suitable EDLC electrode to be combined with N-CNPipes in a LIC.

Full cell of N-CNPipes//PRGO Li-ion capacitor (LIC)

N-CNPipes and PRGO electrodes operate reversibly in different and complementary potential windows (0.01 to 3 V (vs Li/Li^+) and 1.5 V to 4.5 V, respectively (vs Li/Li^+) with different electrochemical mechanisms as shown in Figure 5 (a). This complementarity should naturally lead to a wide working voltage range. Prior to the fabrication of the LIC cell, both N-CNPipes and PRGO electrodes were pre-activated for 10 cycles at 0.25 A/g in Li-half cells. Moreover, N-CNPipes electrode was fully charged (lithiated) up to 0.01 V (vs. Li) to allow for optimal working

of the final device. The mass ratio of PRGO to N-CNPipes was calculated by balancing charges in cathode and anode [50, 51]. The electrochemical performances of N-CNPipes//PRGO LIC cell was tested within the voltage range 0.01-4.0 V. Notably, CV curves at various scan rates show a slight deviation from an ideal capacitive shape, indicating combined contribution from two different charge storage mechanisms (see S.I. S12). Figure 5 (b) shows GCD curves at different current densities from 0.45 A/g to 9 A/g. It is noted that the shapes of GCD curves are not strictly linear, suggesting again that the N-CNPipes//PRGO LIC exhibited combined charge storing mechanisms of a supercapacitor and a battery in agreement with CV results. Figure 5 (c) shows a charge/discharge curve for N-CNPipes//PRGO LIC cell at 1.8 A/g with the corresponding potential profiles measured for cathode and anode (blue and red curves, respectively). As expected, the anode and cathode electrodes work in the voltage ranges: 0.01 V to 2.0 V and 2.0 V to 4.0 V (vs Li/Li^+). The variations of specific capacitance and specific capacity with current densities are shown in Figure 5 (d). The capacity was found to be 168 mAh/g, considering the weight of cathode material which suggests almost 100% utilization of PRGO cathode (by comparison with half-cell). The total capacity was calculated to be 154 mAh/g, considering total weight of active materials in both electrodes (see S. I. S13).

An extended cycling test was carried out at 0.9 A/g for 4000 charge/discharge cycles and its results are presented in Figure 6 (a). Surprisingly, the specific capacity improves during the initial 900 cycles and then starts to decrease slowly until 4000 cycles. The initial increase in the capacity might be due to the activation of functional groups and/or interaction between N-doping in CNPipes. It is further worth noting that the LIC cell retains 91 % of its initial capacity after 4000 cycles, thereby confirming excellent reversibility and cycle life. Moreover, N-CNPipes//PRGO LIC cell exhibits outstanding Coulombic efficiency of 96-98 % over 4000 cycles. A Ragone plot is the graphical representation of the balance between energy and power density, which is key for many practical applications (see S. I. 14).

The Ragone plot of the N-CNPipes//PRGO LIC cell is shown in Figure 6 (b). On the high-energy corner of the ring, our system can deliver ultrahigh energy density of 262 Wh/kg (65.5 Wh/kg considering the weight of full device) at a power density of 450 W/kg which is better than state of the art LIBs [52, 53]. On the high power corner, the N-CNPipes//PRGO LIC can still deliver an energy density of 78 Wh/kg at 9000 W/kg, a combination that surpasses most supercapacitors in terms of energy density [54]. The power and energy of this N-CNPipes//PRGO LIC are even competitive with the best performing LICs energy storage devices reported [14, 55-62], which have triggered considerable recent interest in the literature. As far as we know, ours is the highest value of energy density at high power density for LIC (see S.I. Table 2). SEM analysis of N-CNPipes and PRGO after 1000 charge/discharge cycles was performed (S.I. S15). Remarkably, N-CNPipes maintained their nanotubular structure while PRGO nanosheets were somewhat changed (covered with SEI layer) but still maintained their basic structure. These results confirm that N-CNPipes and PRGO are outstanding anode and cathode materials respectively for LICs.

We have designed an advanced novel LIC with suitable LIB-type anode (N-CNPipes) and capacitor-type cathode (PRGO) which can surpass the main intrinsic drawbacks of kinetics and capacity mismatch in such a combined system. This ultrahigh performance of N-CNPipes//PRGO LIC is credited to the following factors: (i) fast surface reactions involved in both anode (N-CNPipes) and cathode (PRGO) electrodes, (ii) high content of nitrogen (up to 12.5 at.%) into carbon nanopipes facilitates higher electrical conductivity as well as large amount of defect sites which offer extra Li-ion storage (iii) In addition, huge inner space (45 nm) and very thin walls (17-19 nm) of N-CNPipes provide extra-space and short diffusion paths for Li-ion (iv) Moreover, these ultralong open-ended N-CNPipes are endowed with outstanding electrochemical properties such as high reversible capacity, excellent rate capability and long-term cycle-life (v) In addition, 3D open-porous and interconnected nanosheets PRGO provides a conductive network, high surface area, short diffusion lengths which are optimal for

adsorption/desorption of electrolyte ions, thereby providing both improved energy and power densities.

4. Conclusions

In summary, a very high performance LIC fully based on nanocarbon electrodes has been designed and implemented. It is based on a 3D open-porous interconnected partially reduced graphene oxide (PRGO) cathode and ultralong open-end nitrogen-doped carbon nanopipes (N-CNPipes) anode in an organic Li electrolyte to realize simultaneously high energy and power densities. This unique N-CNPipes//PRGO LIC device overcomes the limitations of conventional LIBs and SCs. This device features a high working voltage range up to 4 V, thereby providing ultrahigh energy density of 262 Wh/kg at 450 W/kg and high power density of 9000 W/kg at 78 Wh/kg energy density. Impressively, the energy and power densities obtained in the present work could meet the power demands of the PNGV (Partnership for a New Generation of Vehicles) by providing simultaneously high energy and power densities at low cost.

Acknowledgments

Partial funding from Miisterio de Economía y Competitividad through Fondo Europeo de Desarrollo Regional (FEDER) (Grant MAT2015-68394-R, MINECO/FEDER) and from AGAUR (project NESTOR) are acknowledged. ICN2 acknowledges support of the Spanish MINECO through the Severo Ochoa Centers of Excellence Program under Grant SEV-2013-0295. Finally, the award to DPD of a Marie-Curie Fellowship through Beatriu de Pinos Program (BP-DGR-2013) from the Catalan system of science and technology, Spain, is gratefully acknowledged. DPD acknowledges the support of University of Adelaide, Australia for grant of Research Fellowship (VC Fellow)

References

[1] Y. Gogotsi, P. Simon, *Science*, **2011**, *334*, 917

[2] A. S. Aricò, P. Bruce, B. Scrosati, J. M. Tarascon, W. Van Schalkwijk, *Nat. Mater.* **2005**, *4*, 366

[3] M. R. Palacin, *Chem. Soc. Rev.*, **2009**, *38,* 2565

[4] M. Armand, J. M. Tarascon, *Nature*, **2008**, *451*, 652

[5] F. Bonaccorso, L. Colombo, G. Yu, M. Stoller, V. Tozzini, A. C. Ferrari, R. S. Ruoff, V. Pellegrini, *Science*, **2015**, *347*, 1246501

[6] K. Naoi, W. Naoi, S. Aoyagi, J. Miyamoto, T. Kamino, *Acc. Chem. Res.*, **2013,** *46*, 1075.

[7] D. P. Dubal, O. Ayyad, V. Ruiz, P. Gómez-Romero, *Chem. Soc. Rev.* **2015***, 44*, 1777.

[8] K. Naoi, S. Ishimoto, J. Miyamoto, W. Naoi, *Energy Environ. Sci.* **2012,** *5*, 9363.

[9] V. Aravindan, J. Gnanaraj, Y. S. Lee, S. Madhavi, *Chem. Rev.* **2014,** *114*, 11619.

[10] Y. Ma, H. Chang, M. Zhang, Y. Chen, Y. *Adv. Mater.* **2015**, *27*, 5296.

[11] Z. L. Wang, R. Guo, L. X. Ding, Y. X. Tong, G. R. Li, *Sci. Rep.* **2013**, *3*, 1204.

[12] K. H. An, W. S. Kim, Y. S. Park, J.-M. Moon, D. J. Bae, S. C. Lim, Y. S. Lee, Y. H. Lee *Adv. Funct. Mater.* **2001,** *11*, 387.

[13] M. Winter, R. J. Brodd, *Chem. Rev.* **2004**,*104*, 4245.

[14] H. Kim, H. D. Lim, S. W. Kim, J. Hong, D. H. Seo, D. Kim, S. Jeon, S. Park, K. Kang *Sci. Rep.* **2013,** *3*, 1506

[15] H. Kim, K. Y. Park, J. Hong, K. Kang, *Sci. Rep.* **2014,** *4*, 5278

[16] W. H. Shin, H. M. Jeong, B. G. Kim, J. K. Kang, J. W. Choi, *Nano Lett.* **2012,** *12*, 2283.

[17] X. Li, J. Liu, Y. Zhang, Y. Li, H. Liu, X. Meng, J. Yang, D. Geng, D. Wang, R. Li, X. Sun, *J. Power Sources* **2012,** *197*, 238.

[18] D. Y. Zhong, G. Y. Zhang, S. Liu, E. G. Wang. *Appl. Phys. Lett.* **2001**, *7*, 3500

[19] H. Kim, M. Y. Cho, M. H. Kim, K. Y. Park, H. Gwon, Y. Lee, K. C. Roh, K. Kang, *Adv.*

Energy Mater. **2013**, *3*, 1500.

[20] X. Yang, Z. Zhu, T. Dai, Y. Lu, *Macromol. Rapid Commun.* **2005**, *26*, 1736.

[21] D. P. Dubal, N. R. Chodankar, Z. Caban-Huertas, F. Wolfart, M. Vidotti, R. Holze, C. D. Lokhande, P. Gomez-Romero *J. Power Sources* **2016,** *308*, 158.

[22] H. Ago, T. Kugler, F. Cacialli, W. R. Salaneck, M. S. P. Shaffer, A. H. Windle, R. H. Friend, *J. Phys. Chem. B* **1999,** *103*, 8116.

[23] H. Liu, Y. Zhang, R. Li, X. Sun, S. Desilets, H. Abou-Rachid, M. Jaidann, L. S. Lussier. *Carbon* **2010**, *48*, 1498.

[24] G. Kaushik, K. Mukul, M. Takahiro, A. Yoshinori, *J. Mater. Chem.* **2010,** *20*, 4128.

[25] L. G. Bulusheva, A. V. Okotrub, A. G. Kurenya, H. Zhang, H. Zhang, X. Chen, H. Song, *Carbon* **2011,** *49*, 4013.

[26] F. D. Han, Y. J. Bai, R. Liu, B. Yao, Y. X. Qi, N. Lun, J. X. Zhang, *Adv. Energy Mater.* **2011**, *1*, 798.

[27] B. J. Landi, M. J. Ganter, C. D. Cress, R. A. DiLeo, R. P. Raffaelle, *Energy Environ. Sci.* **2009,** *2*, 638.

[28] NIST X-ray Photoelectron Spectroscopy Database, Version 4.1 (National Institute of Standards and Technology (2012); http://srdata.nist.gov/xps/.

[29] R. Mukherjee, A. V. Thomas, D. Datta, E. Singh, J. Li, O. Eksik, V. B. Shenoy, N. Koratkar, *Nat. Commun.* **2014,** *5*, 3710.

[30] D. Lin, Y. Liu, Z. Liang, H. W. Lee, J. Sun, H. Wang, K. Yan, J. Xie, Y. Cui, *Nat. Nanotech.* **2016,** *11*, 626.

[31] K. Yan, Z. Lu, H. W. Lee, F. Xiong, P. C. Hsu, Y. Li, J. Zhao, S. Chu, Y. Cui. *Nat. Energy* **2016,** *1*, 16010

[32] Z. W. She, H. Wang, P. C. Hsu, Q. Zhang, W. Li, G. Zheng, H. Yao, Y. Cui, *Energy Environ. Sci.*, **2014,** *7*, 672.

[33] G. Cherkashinin, K. Nikolowski, H. Ehrenberg, S. Jacke, L. Dimesso, W. Jaegermann, *Phys. Chem. Chem. Phys.*, **2012,** *14*, 12321.

[34] B. Kang, G. Ceder *Nature* **2009,** *458*, 190.

[35] F. M. Hassan, R. Batmaz, J. Li, X. Wang, X. Xiao, A. Yu, Z. Chen *Nat. Commun.* **2015**, *6*, 8597

[36] Z. J. Fan, J. Yan, T. Wei, G. Q. Ning, L. J. Zhi, J. C. Liu, D. X. Cao, G. L. Wang, F. Wei, *ACS Nano* **2011,** *5*, 2787.

[37] V. G. Pol, M. M. Thackeray, *Energy Environ. Sci.* **2011**, *4*, 1904.

[38] Z. Chen, V. Augustyn, X. Jia, Q. Xiao, B. Dunn, Y. Lu, *ACS Nano* **2012**, *6*, 4319.

[39] N. Gavrilov, I. A. Pasti, M. Vujkovic, J. Travas-Sejdic, G. Ciric-Marjanovic, S. V. Mentus S. V. *Carbon* **2012,** *50*, 3915.

[40] L. Qie, W. M. Chen, Z. H. Wang, Q. G. Shao, X. Li, L. X. Yuan, X. L. Hu, W. X. Zhang, Y. H. Huang, *Adv. Mater.* **2012,** *24*, 2047.

[41] H. G. Jung, J. Hassoun, J. B. Park, Y. K. Sun, B. Scrosati, *Nat. Chem.* **2012,** *4*, 579.

[42] H. Guo, X. Li, X. Zhang, H. Wang, Z. Wang, W. Peng, *New Carbon Mater.* **2007,** *22*, 7.

[43] P. Yu, B. N. Popov, J. A. Ritter, R. E. White, *J. Electrochem. Soc.,* **1999,** *146***,** 8.

[44] A. S. Claye, J. E. Fischer, C. B. Huffman, A. G. Rinzler, R. E. Smalley, *J. Electrochem. Soc.,* **2000,** *147***,** 2845

[45] V. Chabot, D. Higgins, A. Yu, X. Xiao, Z. Chen, J. Zhang *Energy Environ. Sci.,* **2014,** *7*, 1564.

[46] (a) Q. Wang, Z. Wen, J. Li, *Adv. Funct. Mater.* **2006,** *16*, 2141. (b) B. Wang, Q. Wang, B. Xu, T. Liu, D. Wang, G. Zhao, *RSC Adv.*, **2013**, 3, 20024

[47] V. Aravindan, D. Mhamane, W. C. Ling, S. Ogale, S. Madhavi, *ChemSusChem* **2013,** *6,* 2240.

[48] A. Banerjee, K. K. Upadhyay, D. Puthusseri, V. Aravindan, S. Madhavi, S. Ogale

Nanoscale **2014**, *6*, 4387

[49] (a) G. P. Kim, S. Park, I. Nam, J. Park, J. Yi, *J. Power Sources* **2013,** *237*, 172. (b) B. Wang, T. Liu, A. Liu, G. Liu, L. Wang, T. Gao, D. L. Wang, X. S. Zhao, Adv. Energy Mater. 2016, 6, 1600426. (c) B. Wang, A. Liu, W. A. Abdulla, D. Wang, X. S. Zhao, *Nanoscale*, **2015**, 7, 8819-8828

[50] F. Zhang, T. Zhang, X. Yang, L. Zhang, K. Leng, Y. Huang, Y. Chen, *Energy Environ. Sci.* **2013,** *6*, 1623.

[51] A. Jain, V. Aravindan, S. Jayaraman, P. S. Kumar, R. Balasubramanian, S. Ramakrishna, S. Madhavi, M. P. Srinivasan, *Sci. Rep.* **2013,** *3*, 3002.

[52] (a) G. B. Appetecchi, P. P. Prosini, *J. Power Sources* **2005,** *146*, 793. (b) B. Wang, W. A. Abdulla, D. Wang, X. S. Zhao, *Energy Environ. Sci.*, **2015**, 8, 869-875

[53] J. Hassoun, F. Bonaccorso, M. Agostini, M. Angelucci, M. G. Betti, R. Cingolani, M. Gemmi, C. Mariani, S. Panero, V. Pellegrini, B. Scrosati *Nano Lett.*, **2014**, *14*, 4901.

[54] E. Raymundo-Pinero, F. Leroux, F. Beguin, *Adv. Mater.* **2006**, *18*, 1877.

[55] E. Lim, C. Jo, H. Kim, M. H. Kim, Y. Mun, J. Chun, Y. Ye, J. Hwang, K. S. Ha, K. C. Roh, K. Kang, S. Yoon, J. Lee, *ACS Nano* **2015**, *9*, 7497.

[56] H. Kim, M. Y. Cho, M. H. Kim, K. Y. Park, H. Gwon, Y. Lee, K. C. Roh, K. Kang, *Adv. Energy Mater.* **2013**, *3*, 1500.

[57] R. Yi, S. Chen, J. Song, M. L. Gordin, A. Manivannan, D. Wang *Adv. Funct. Mater*. **2014,** *24*, 7433.

[58] H. Wang, C. Guan, X. Wang, H. J. Fan, *Small* **2015,** *11*, 1470.

[59] K. Karthikeyan, S. Amaresh, S. N. Lee, V. Aravindan, Y. S. Lee, *Chem. Asian J.* **2014,** *9*, 852.

[60] K. Leng, F. Zhang, L. Zhang, T. Zhang, Y. Wu, Y. Lu, Y. Huang, Y. Chen, *Nano Res.* **2013,** *6*, 581.

[61] X. Wang, P. S. Lee, *J. Mater. Chem. A,* **2015,** *3*, 21706.

[62] H. Wang, Y. Zhang, H. Ang, Y. Zhang, H. T. Tan, Y. Zhang, Y. Guo, J. B. Franklin, X. L. Wu, M. Srinivasan, H. J. Fan, Q. Yan, *Adv. Funct. Mater.* **2016**, *26*, 3082.

Figure captions

Figure 1 (a and b) Core-level XPS spectra of C1s and N1s for N-CNPipes, respectively. C1s spectrum is deconvulated in three small peaks. (c) FESEM image of N-CNPipes at high magnification, indicating ultra-long nanopipes. (d-e) TEM and HRTEM images of N-CNpipes further assuring the formation of ultra-long, open end nanopipes with low graphitization due to N-doping. (f) EFTEM mapping images of N-CNPipes, suggesting the uniform distribution of carbon and nitrogen

Figure 2 Electrochemical properties of N-CNPipes in Li-half cell configuration (a) Initial four cyclic voltammetry curves recorded at scan rate of 1 mV/s, (b) Initial four charge/discharge curves measured at 1C= 0.5 A/g, (c) variation of capacity with cycling at different rates and (d) Cycling stability and Coulombic efficiency over 1000 cycles at 0.5 A/g, showing capacity retention of 59 % after 1000 cycles.

Figure 3 (a) Schematic illustration of charge storing mechanism involved in the N-CNpipes with corresponding TEM and HRTEM images, (b) Plots of Log(current) versus Log(scan rate) for N-CNPipes electrode in order to determine the *b* -values in the CV curves from 1 to 10 mV/s. (c) The contribution from capacitive and diffusion controlled charge storage in N-CNPipes electrode at different scan rates, (d) Li-ion diffusion coefficients at different scan rates

Figure 4 (a) FESEM of PRGO, showing highly porous, interconnected nanosheets network, inset shows TEM image of PRGO nanosheets. (b-c) Electrochemical properties of partially

reduced graphene oxide (PRGO) electrode in a Li half-cell within the potential range of 1.5 to 4.5 V (vs Li/Li^+). (b) Galvanostatic charge/discharge curves at different rates, (c) Rate capability properties of PRGO at different current densities, (d) Cycle life performance and Coulombic efficiency measured over 5000 cycles at 0.34 A/g

Figure 5 Electrochemical properties of N-CNPipes//PRGO LIC full cell in voltage range of 0.01 to 4 V; (a) schematic illustration of design of unique LIC with combined CV curves of N-CNpipes and PRGO in different voltage windows such as +0.01 to 3.0 V and +1.5 V to 4.5 V (vs Li/Li+), respectively, indicating inclusion of different charge storing mechanisms, (b) Typical charge/discharge curves for N-CNPipes//PRGO LIC cell, inset shows magnified view of CD curves at high current densities, (c) CD curve for N-CNPipes//PRGO LIC cell at current density of 1.8 A/g with corresponding voltage distribution across N-CNPipes anode and PRGO cathode versus Li-foil reference electrode, (d) Variation of specific capacitance and capacity with current density for N-CNPipes//PRGO LIC cell.

Figure 6 (a) Capacity retention and Coulombic efficiency of N-CNPipes//PRGO LIC cell over 1000 cycles, suggesting excellent cycling stability with >95 % Coulombic efficiency. (b) Ragone plot for N-CNPipes//PRGO LIC device with comparison of previously reported values.

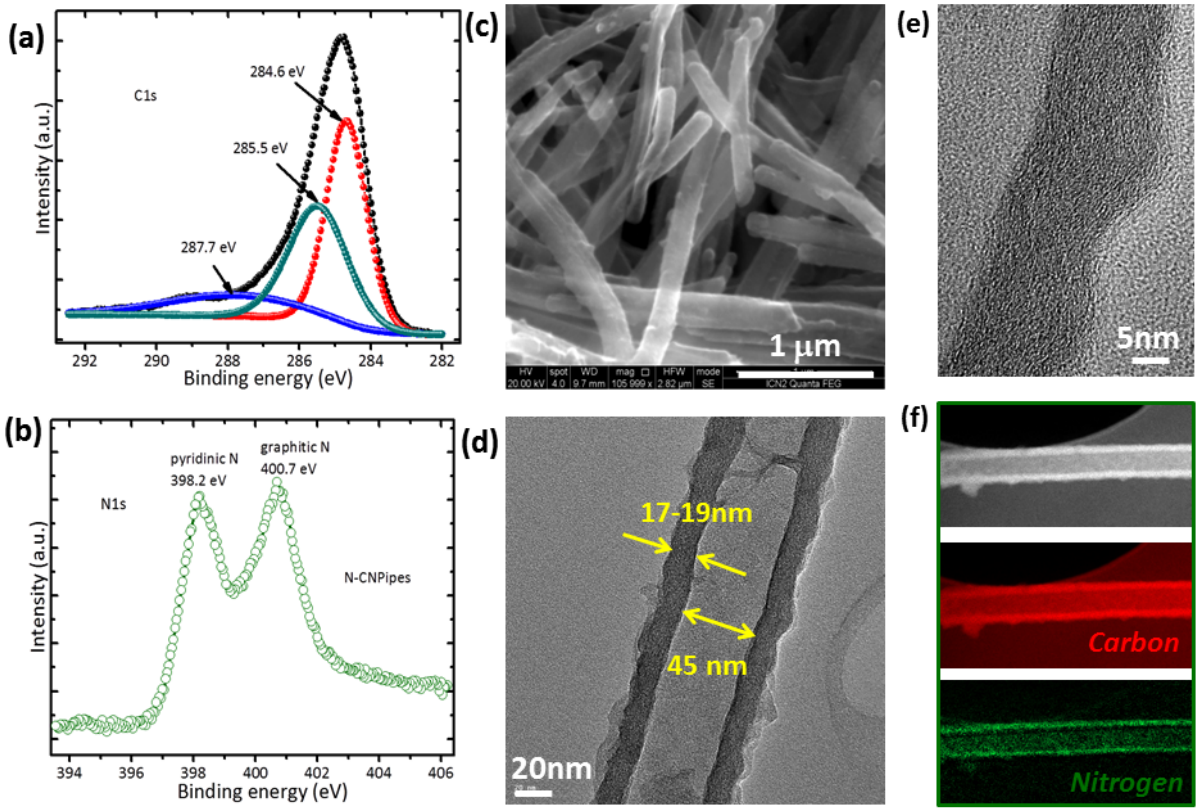
(a)
C1s
284.6 eV
285.5 eV
287.7 eV
Intensity (a.u.)
292
290
288
286
284
282
Binding energy (eV)
(b)
N1s
pyridinic N
398.2 eV
graphitic N
400.7 eV
N-CNPipes
Intensity (a.u.)
394
396
398
400
402
404
406
Binding energy (eV)
(c)
1 µm
(d)
17-19nm
45 nm
20nm
(e)
5nm
(f)
Carbon
Nitrogen

Figure 1

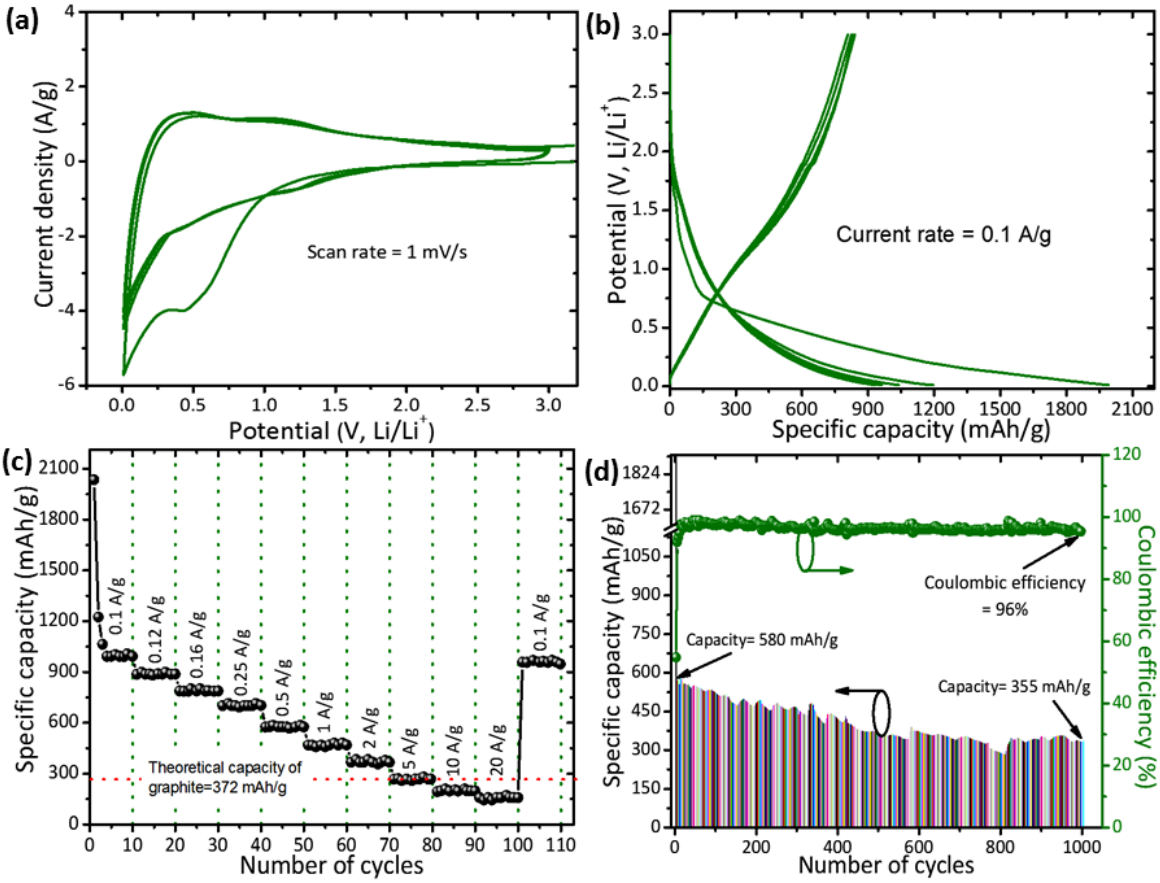
(a)
Current density (A/g)
Potential (V, Li/Li+)
Scan rate = 1 mV/s
(b)
Potential (V, Li/Li+)
Specific capacity (mAh/g)
Current rate = 0.1 A/g
(c)
Specific capacity (mAh/g)
Number of cycles
0.1 A/g
0.12 A/g
0.16 A/g
0.25 A/g
0.5 A/g
1 A/g
2 A/g
5 A/g
10 A/g
20 A/g
0.1 A/g
Theoretical capacity of graphite=372 mAh/g
(d)
Specific capacity (mAh/g)
Coulombic efficiency (%)
Number of cycles
Coulombic efficiency = 96%
Capacity= 580 mAh/g
Capacity= 355 mAh/g

Figure 2

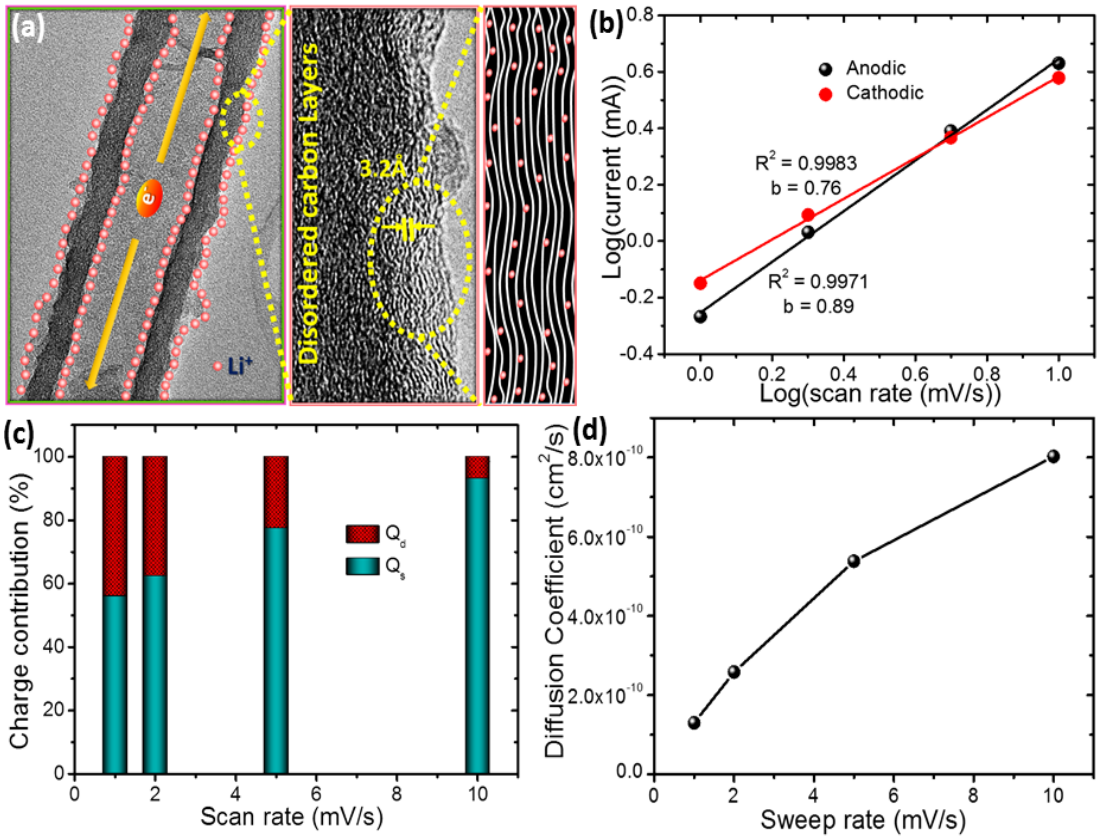
(a)
e⁻
Li⁺
Disordered carbon layers
0.2 nm
(b)
Anodic
Cathodic
R² = 0.9983
b = 0.76
R² = 0.9971
b = 0.89
Log(current (mA))
Log(scan rate (mV/s))
(c)
Q_d
Q_s
Charge contribution (%)
Scan rate (mV/s)
(d)
Diffusion Coefficient (cm²/s)
Sweep rate (mV/s)

Figure 3

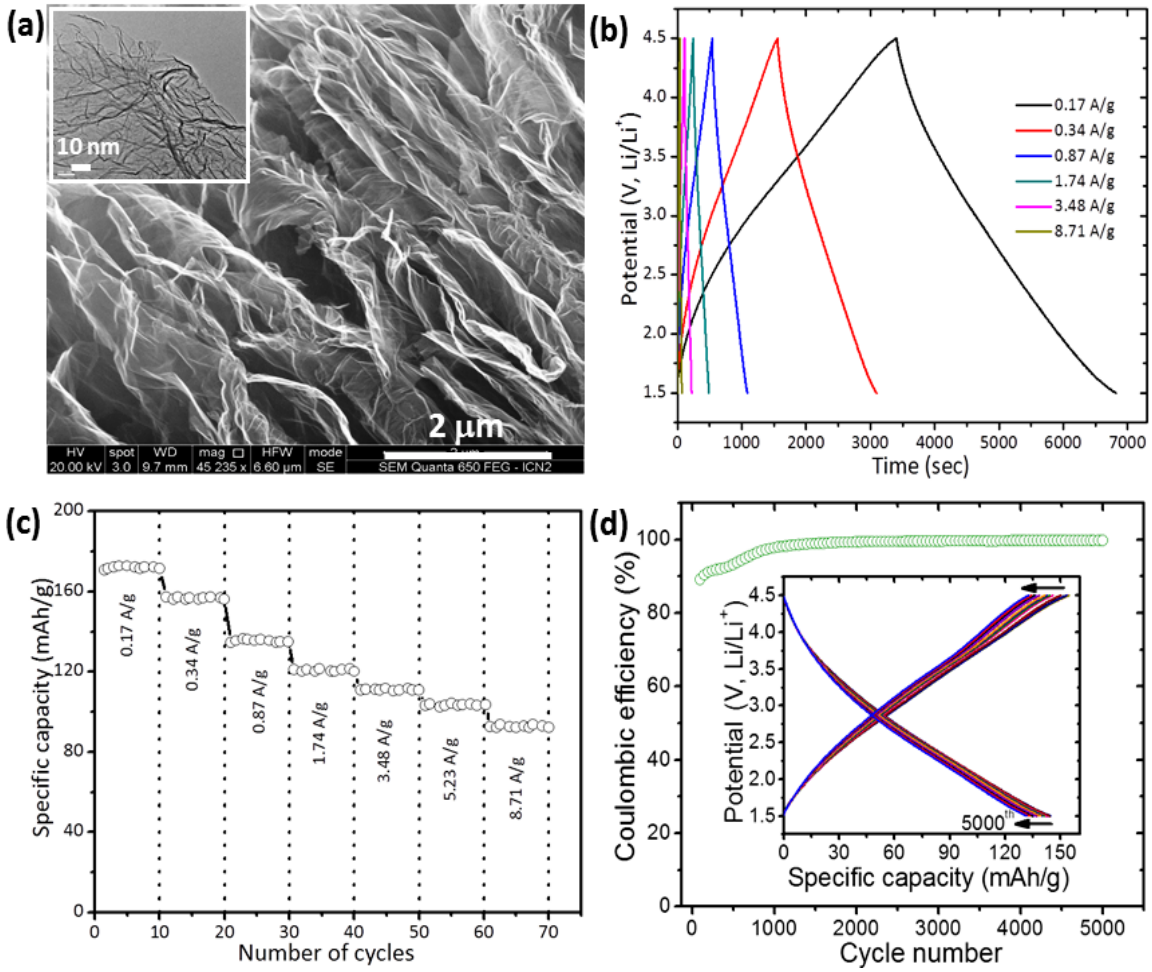
(a)
10 nm
2 µm
HV spot WD mag HFW mode
20.00 kV 3.0 9.7 mm 45 235 x 6.60 µm SE
SEM Quanta 650 FEG - ICN2
(b)
Potential (V, Li/Li+)
Time (sec)
0.17 A/g
0.34 A/g
0.87 A/g
1.74 A/g
3.48 A/g
8.71 A/g
(c)
Specific capacity (mAh/g)
Number of cycles
0.17 A/g
0.34 A/g
0.87 A/g
1.74 A/g
3.48 A/g
5.23 A/g
8.71 A/g
(d)
Coulombic efficiency (%)
Cycle number
Potential (V, Li/Li+)
Specific capacity (mAh/g)
5000th

Figure 4

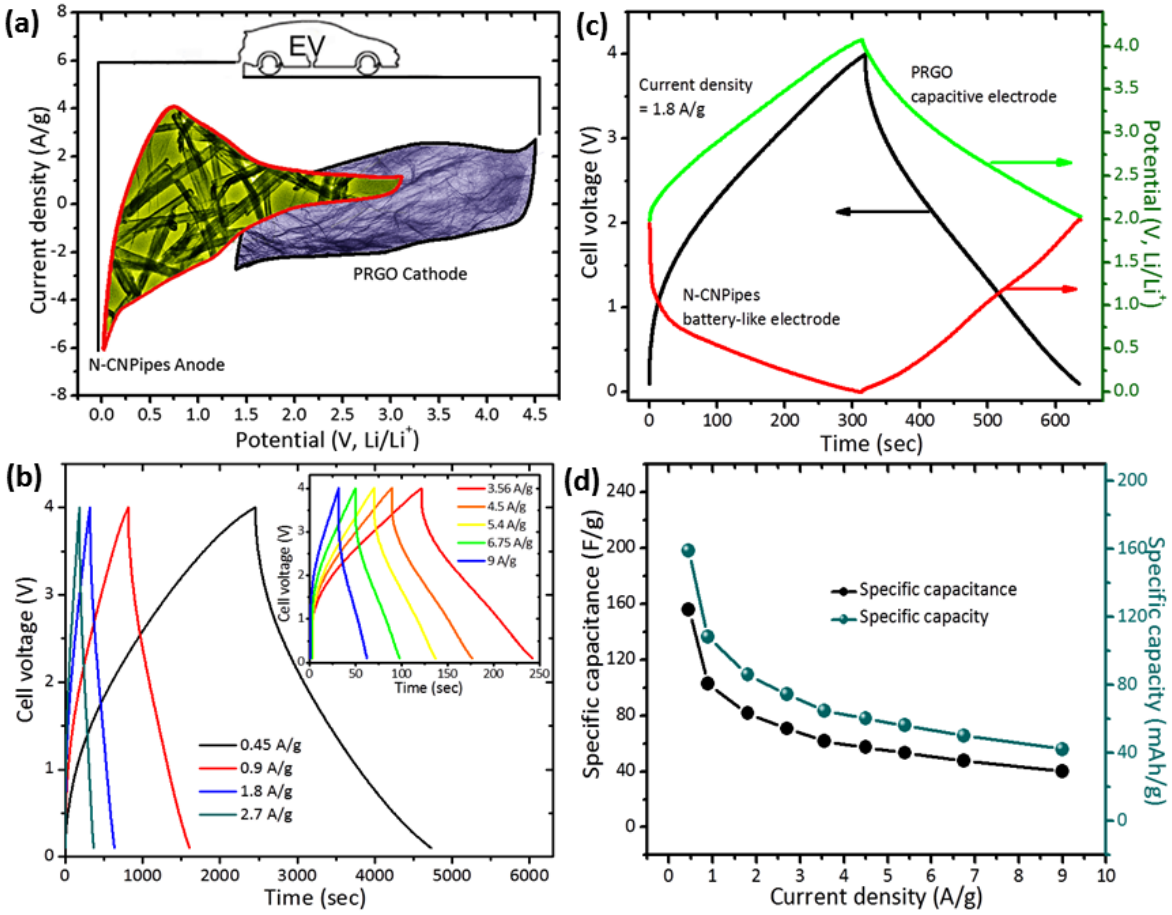
(a)
EV
Current density (A/g)
Potential (V, Li/Li+)
PRGO Cathode
N-CNPipes Anode
(c)
Current density
= 1.8 A/g
PRGO
capacitive electrode
N-CNPipes
battery-like electrode
Cell voltage (V)
Potential (V, Li/Li+)
Time (sec)
(b)
Cell voltage (V)
Time (sec)
0.45 A/g
0.9 A/g
1.8 A/g
2.7 A/g
3.56 A/g
4.5 A/g
5.4 A/g
6.75 A/g
9 A/g
(d)
Specific capacitance (F/g)
Specific capacity (mAh/g)
Specific capacitance
Specific capacity
Current density (A/g)

Figure 5

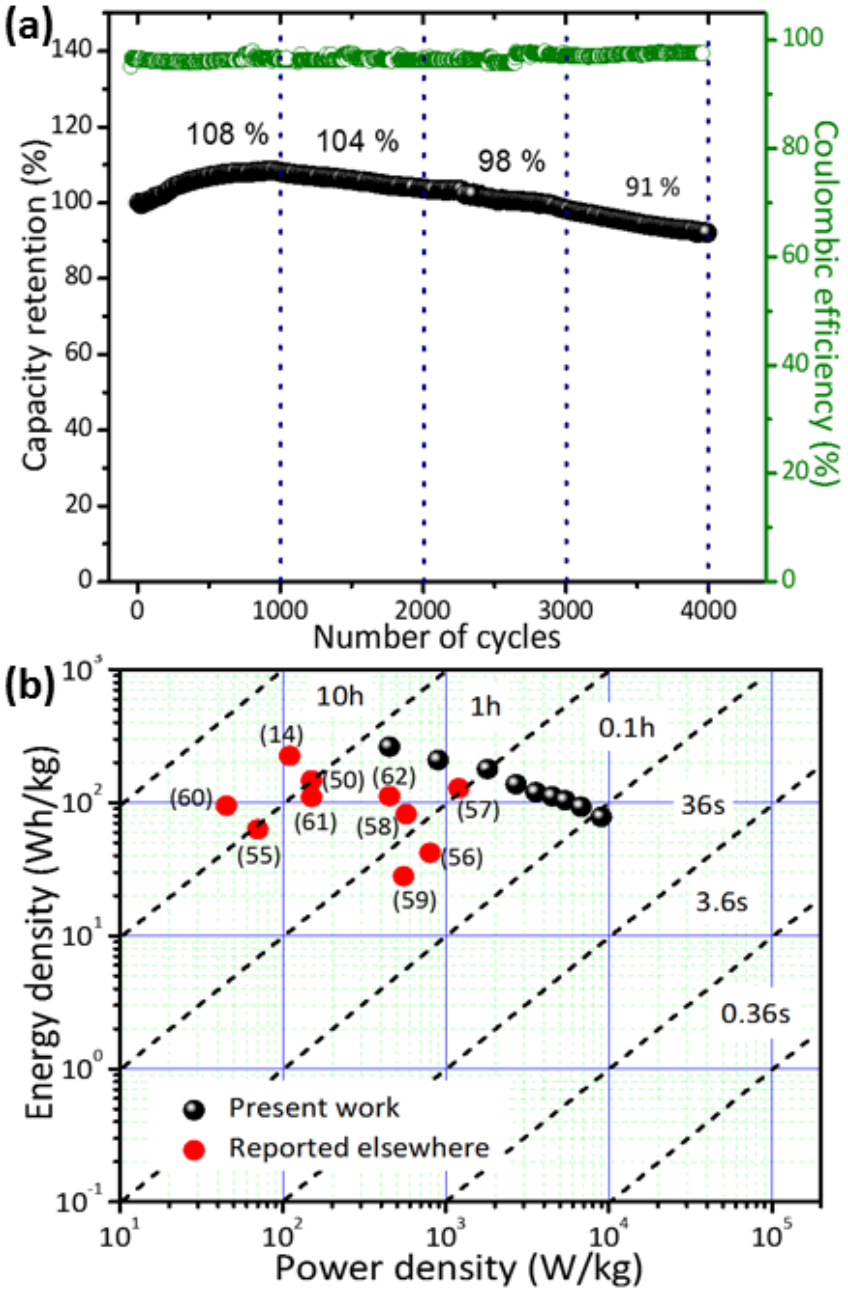
(a)
Capacity retention (%)
Coulombic efficiency (%)
Number of cycles
108 %
104 %
98 %
91 %
(b)
Energy density (Wh/kg)
Power density (W/kg)
10h
1h
0.1h
36s
3.6s
0.36s
(14)
(60)
(50)
(62)
(61)
(58)
(57)
(55)
(56)
(59)
Present work
Reported elsewhere

Figure 6

The table of contents

The complementary electrochemistries of two different but ***kinetically balanced*** nanocarbons (Carbon Nano-Pipes and Partially Reduced Graphene Oxide) (left) can be combined in a breakthrough Li-Ion Capacitor device (LIC) featuring ***simultaneously*** high specific power and energy (right).

Keywords: Nanocarbon, Li-ion capacitor, High energy density

Deepak P. Dubal,[a, b] Pedro Gomez-Romero [b]**

All Nanocarbon Li-Ion Capacitor with High Energy and High Power Density

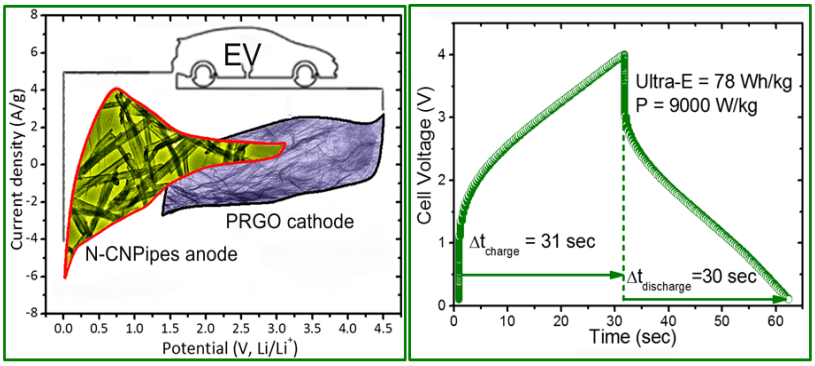

Supporting Information

All Nanocarbon Li-Ion Capacitor with High Energy and High Power Density

Deepak P. Dubal,[a, b] Pedro Gomez-Romero [a]**

Supporting Information S1

Methods

Synthesis of N-doped carbon nanopipes (N-CNPipes) anode

The N doped carbon nanopipes (N-CNPipes) are prepared from the pyrolysis of popypyrrole nanopipes as described in previous report [1]. Briefly, 0.15 mmoles (0.049 g) of Methyl Orange (MO) (i.e. sodium 4-[40 (dimethylamino)phenyldiazo]phenylsulfonate ($(CH_3)_2NC_6H_4$-N=$NC_6H_4SO_3Na$)) and 1.5 mmoles $FeCl_3$ (0.243 g) were dissolved in 30 ml de-ionized water and maintained stirring for 20 min, forming a flocculent precipitate. Later, 105 μL (1.5 mmoles) pyrrole was mixed to the above solution and the mixture was kept stirring at room temperature for 24 h. The obtained product was then filtered and repeatedly washed with mixture of distilled water and ethanol and finally dried overnight under vacuum at 80 °C. For the preparation of N doped carbon nanopipes (N-CNPipes), a small amount of PPy-NPipes were heat-treated at 800 °C with a heating rate of 5 °C/min for 1 h, under N_2 atmosphere.

Synthesis of partially reduced graphene oxide (PRGO) cathode

To begin with, graphene oxide (GO) was first prepared by modified Hummers method described as follows. 2.5 g of graphite powder was added to the mixture of 2.5 g sodium nitrate ($NaNO_3$) and 110 ml sulfuric acid (H_2SO_4) and the mixture was stirred in an ice bath for 30 min. Later, 12 g of potassium permanganate ($KMnO_4$) was added to the above solution and the solution was maintained at 50 °C for 2 h with constant stirring. Next, 300 ml of deionized water and 15 ml hydrogen peroxide (H_2O_2, 35%) were then gradually added to the solution. Later, the solution was washed with 500 ml of hydrochloric acid (HCl, 10%). Finally, the GO was washed with extra 200 ml HCl (37%) and deionized water and then dried in vacuum oven at 60 °C overnight. In order to prepare partially reduced graphene oxide (FGO), the GO powder was annealed at 120 °C for 6 h.

Materials characterization

The surface morphological analyses of samples were carried out using the different techniques such as field-emission scanning electron microscopy (FEI Quanta 650F Environmental SEM) attached with an energy-dispersive X-ray spectroscopy (EDS) analyzer to measure the sample composition and transmission electron microscopy (Tecnai G2 F20 S-TWIN HR(S) TEM, FEI). The crystal structure analysis was performed with Panalytical X'pert Pro-MRD instrument (Cu Ka radiation and PIXel detector). The X-ray photoelectron spectra (XPS) analyses were obtained by X-ray photoelectron spectroscopy (XPS, SPECS Germany, PHOIBOS 150). N2 adsorption/desorption was determined by Brunauer-Emmett-Teller (BET) measurements using Micromeritics instrument (Data Master V4.00Q, Serial#:2000/2400).

Electrochemical testing

Electrodes were prepared by mixing the active material (partially reduced graphene oxide, PRGO or N-doped carbon nanopipes, N-CNPipes), Super-P conductive carbon black and polyvinylidene fluoride binder (PVDF) in an N-methyl-2-pyrrolidone (NMP) with 80 %:10 %:10% ratio. The resulting paste was uniformly coated onto Al or Cu foil, dried at 100 °C for 12 h, and pressed under hydraulic press. The mass loading of N-CNPipes and PRGO was around 2-2.5 mg. Initially, both the materials PRGO and N-CNPipes were tested with half-cell configuration where the Li metal, glass-fiber and a 1 M lithium hexafluorophosphate in a 1:1 mixture of ethylene carbonate and dimethyl carbonate (1:1, EC:DMC) were used as counter electrode, separator and electrolyte, respectively. The PRGO cathode half-cell was tested within the voltage range from 4.5 to 1.5 V and N-CNPipes anode within 3.0 to 0.01 V using a Biologic potentio-galvanostat. Prior to assembling full LIC cell, N-CNPipes and PRGO were cycled 10 cycles in half-cells at 0.5 A/g, and then the cells were disassembled in the glove box and by collecting electrodes, full cell was fabricated and tested within 0.01 to 4 V. The N-CNPipes anode was fully discharged up to 0.01 V (vs. Li) before used in the full LIC cells. In present

investigation, the mass ratio of N-CNPipes to PRGO was maintained at 1:8 (1.3 mg of N-CNPipes and 9.8 mg of PRGO).

Supporting Information S2

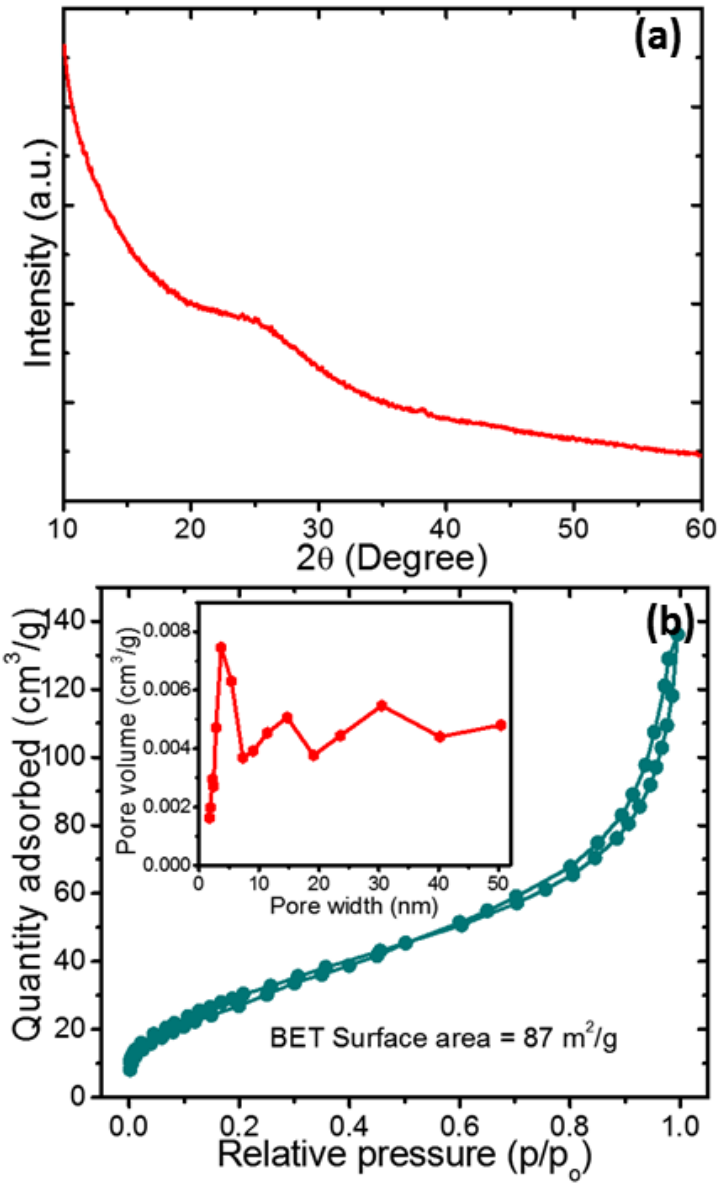

Figure S2 (a, b) XRD and Nitrogen adsorption/desorption isotherm of N-CNPipes, respectively, Inset of Fig. (b) shows the corresponding pore size distribution.

Supporting Information S3

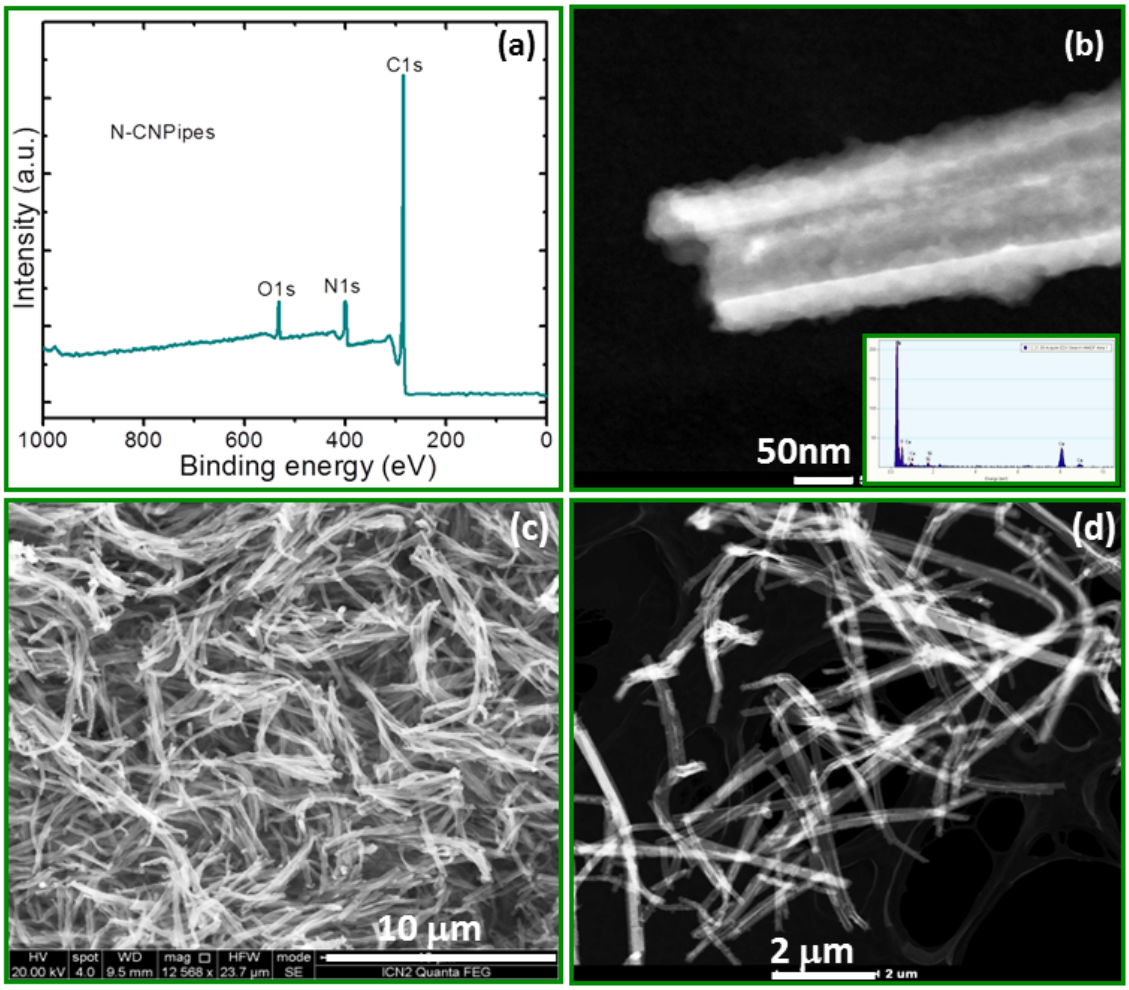

Figure S3 (a) Full XPS spectrum of N-CNPipes, showing the presence of C, N and O (b) high magnified EFTEM image, showing open and low graphitic texture of nitrogen-doped carbon nanopipes (c, d) low magnified FESEM and EFTEM images confirming the formation of ultra-long nitrogen-doped carbon nanopipes.

Supporting Information S4

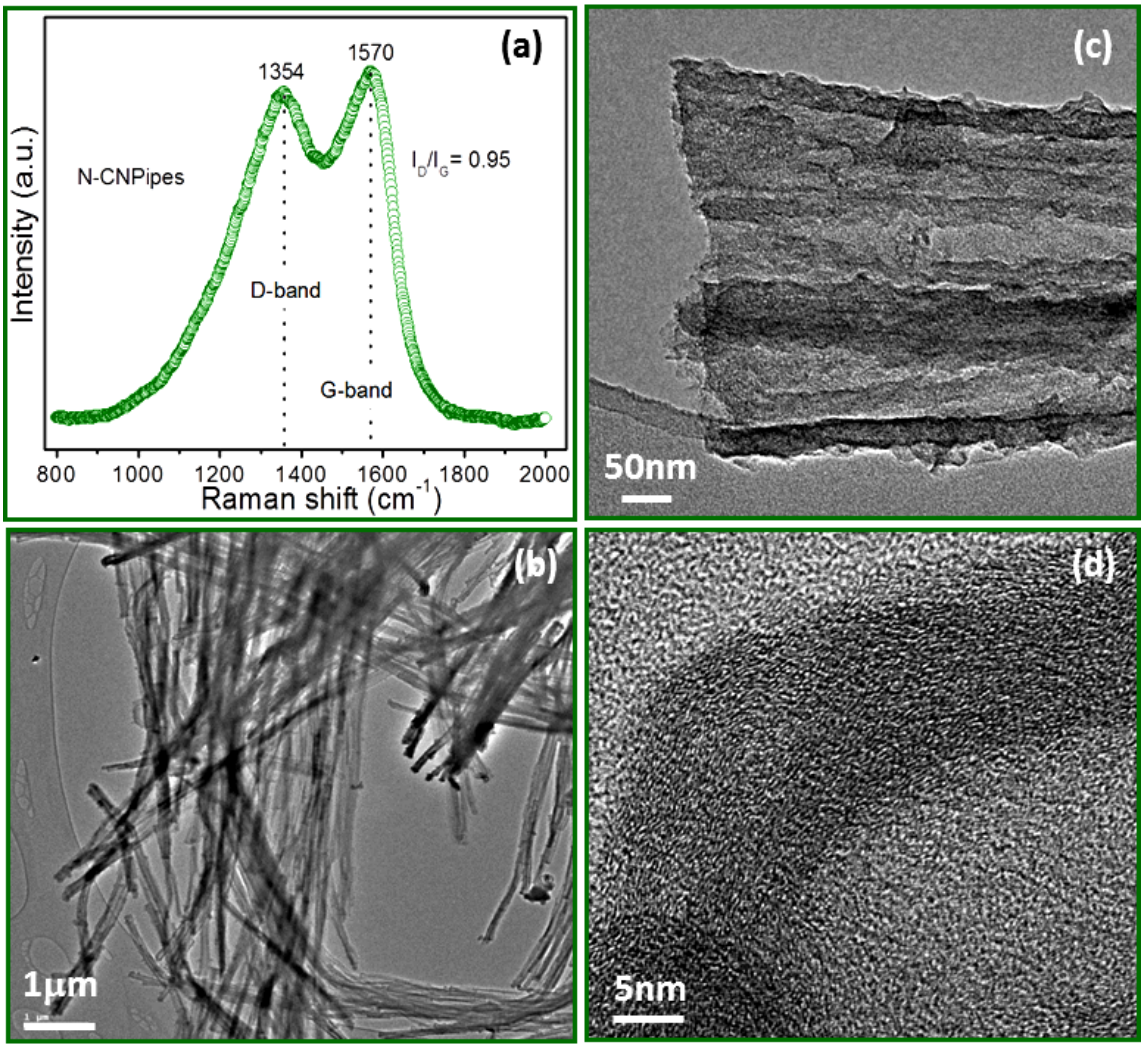

Figure S4 (a) Raman spectrum of N-CNPipes, showing I_G/I_D ratio of around 0.96 indicating the formation of high quality carbon nanopipes, (b-d) TEM and HRTEM images of N-CNPipes suggesting lengths of nanopipes of a few micrometers, open-end and low graphitization due to nitrogen doping.

Supporting Information S5

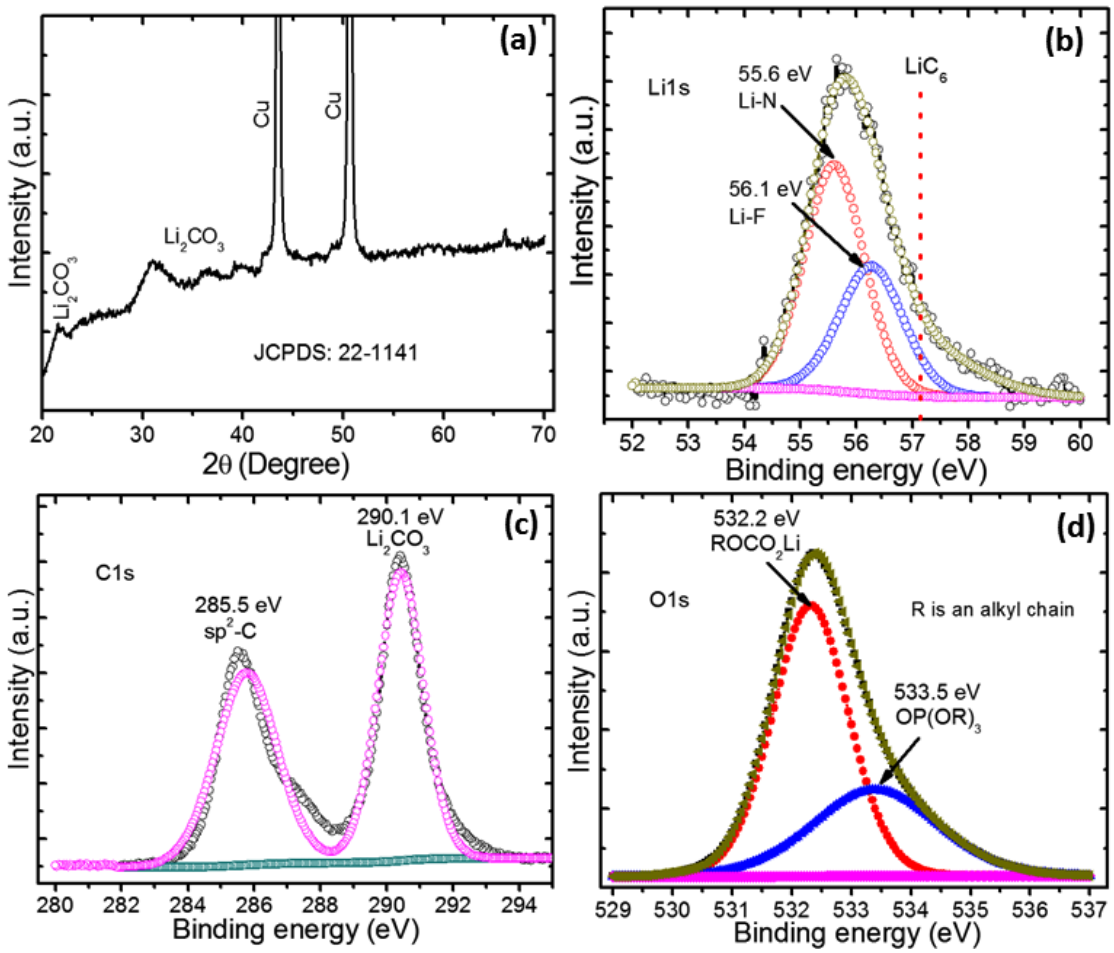

Figure S5 (a) XRD pattern of N-CNPipes after 1000 charge/discharge cycles, showing the formation of SEI layer (Li_2CO_3). (b-d) Core-level XPS spectra of Li1s, C1s, and O1s for N-CNPipes after 1000 cycles, respectively.

The formation of a solid electrolyte interface (SEI) after electrochemical cycling is confirmed from XRD pattern as well as C1s and O1s spectra which arises due to the deterioration of the electrolyte and electrode due to surface reactions. The peak observed in C1s spectrum at binding energy of 290.1 eV corresponds to the Li_2CO_3 while two deconvoluted peaks observed in O1s spectrum might be associated to lithium alkyl carbonates ($ROCO_2Li$, 532.2 eV) resulting from the decomposition of DMC and phosphor-containing species like $OP(OR)_3$ with binding energy of 533.5 eV (where R is an alkyl chain).

Supporting Information S6

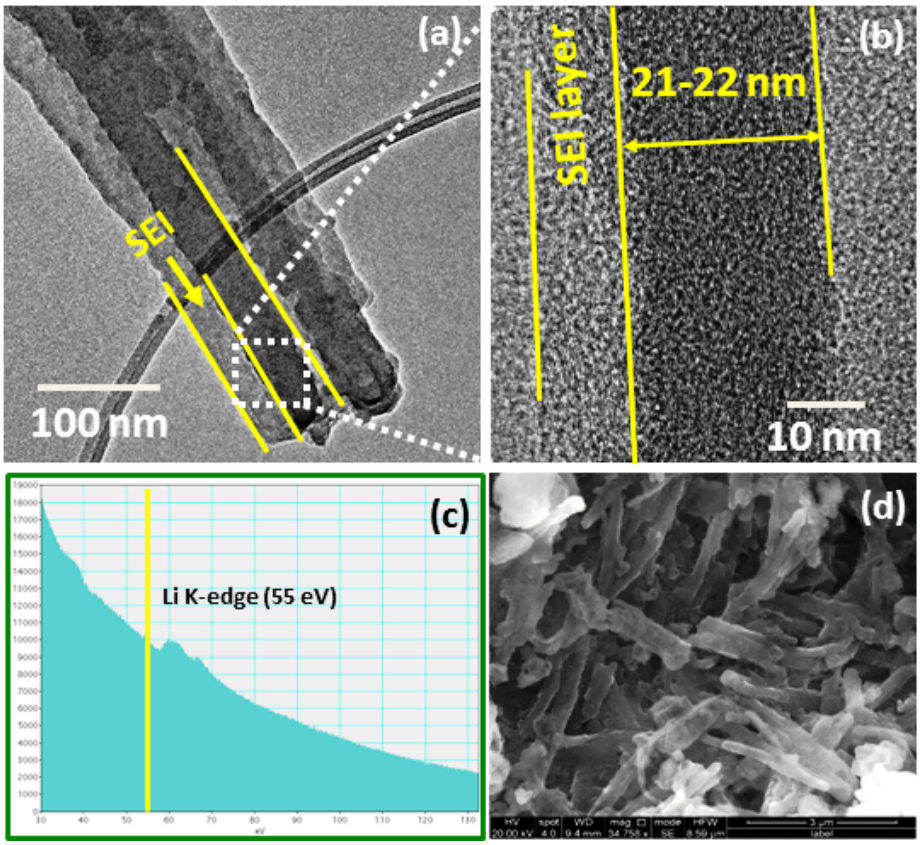

Figure S6 (a) TEM, HRTEM and SAED images of N-CNPipes after 1000 charge/discharge cycles in half cell configuration, indicating the formation of SEI layer. Moreover, due to the Li storage in interwall space the size of nanopipes is increased from 17-18 nm to 21-22 nm. It is further noticed that there is no sign of dendrite growth on the surface of N-CNPipes (d) SEM image of N-CNPipes after 1000 cycles which shows that N-CNPipes preserve their tubular nanostructure after such a high number of charge/discharge cycles.

Supporting Information S7

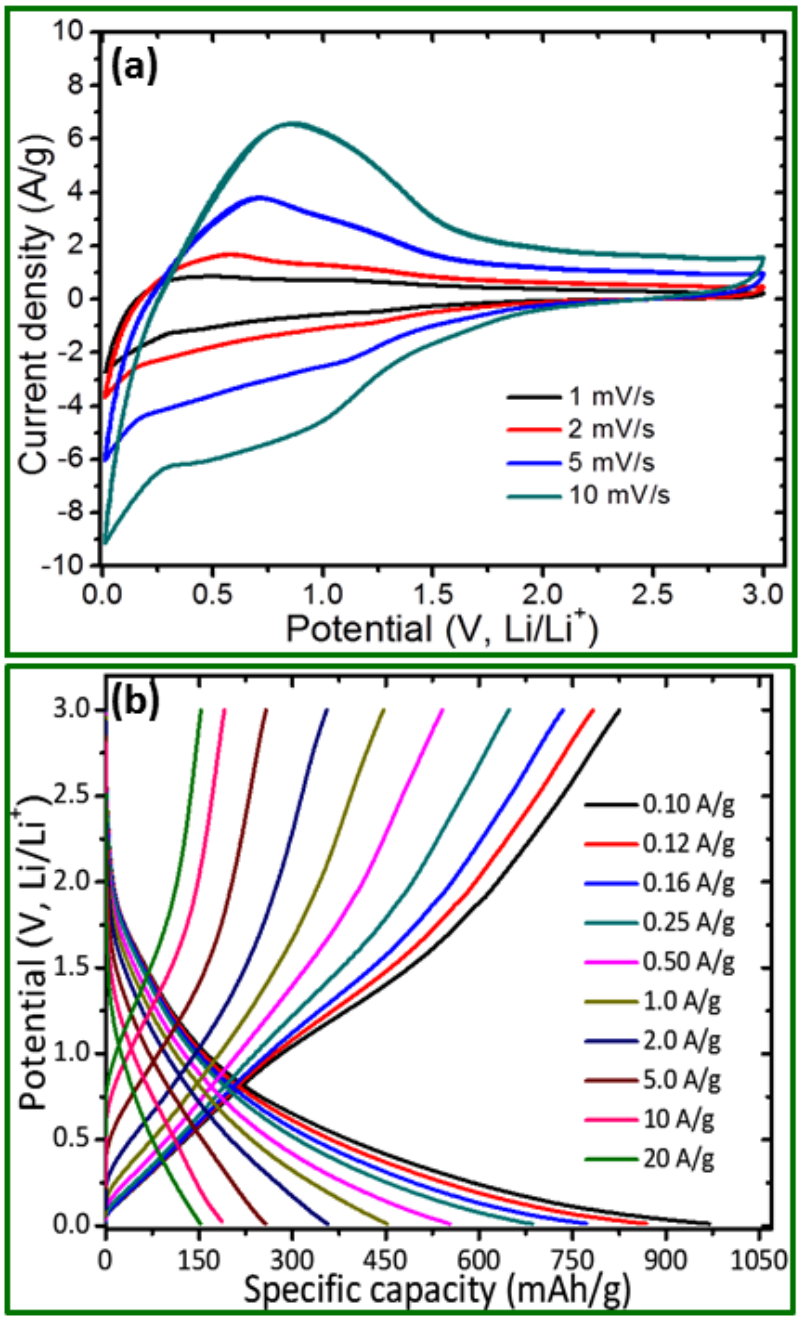

Figure S7 (a) Cyclic voltammetry curves for N-CNPipes at various scan rates. (b) The typical galvanostatic charge/discharge curves for N-CNPipes at different current densities.

Supporting Information Table 1

Table 1 Comparison of electrochemical properties of carbon based anode materials with present report

Anode Material	Reversible capacity (mAh/g)	Capacity retention (mAh/g)	References
N-CNPipes	982 at 0.1 A/g	345 at 0.5 A/g after 1000 cycles	Present work
N-CNTs[1]	494 at 100 mA/g	397 at 100 mA/g after 100 cycles	[S2]
N-CNFs[2]	1280 at 0.1 A/g	943 at 2 A/g after 600 cycles	[S3]
N-CNTs	270 at 0.2 mA/cm^2	270 at 0.2 mA/cm^2 after 30 cycles	[S4]
N-graphene film	0.05 mAh/cm^2 at 5 □μA/cm^2	0.05 mAh/cm^2 at 5 μA/cm^2 after 50 cycles	[S5]
N-CNTs	400 at 80 mA/g	1900 at 80 mA/g after 200 cycles	[S6]
Open ended -CNTs	1080 at 100 mA/g	432 mAh/g at 100 mA/g after 50 cycles	[S7]
Functionalized CNTs	200 at 0.4 A/g	200 mAh/g at 0.25 A/g after 1000 cycles	[S8]
Hollow Carbon-Nanotube /Carbon-Nanofiber	1150 at 0.1 A/g	320 mAh/g at 8 A/g after 3500 cycles	[S9]
(Fe&Fe_3O_4)@PGC[3] nanosheets	722 at 100 mA/g	112 mAh/g at 30 C after 570 cycles (96 % capacity retention)	[S10]
Fe_3O_4-C nanospindles	745 at C/5	530 at C/2 after 80 cycles	[S11]

Boron doped graphene	1040 at 50 mA/g	1227 at 50 mA/g after 80 cycles	[S12]
N-Graphene	1043 at 50 mA/g	873 at 50 mA/g after 80 cycles	[S13]
Graphene-Fe_3O_4	1026 at 35 mA/g	580 at 700 mA/g after 100 cycles	[S14]
Sb/MWCNT[4]	1266 at 50 mA/g	287 at 50 mA/g after 30 cycles	[S15]
TiO_2/MWCNT	830 at 50 mA/g	165 at 50 mA/g after 75 cycles	[S16]
TiO_2/MWCNT	728 at 37.2 mA/cm^2	126.4 at 37.2 mA/cm2 after 40 cycles	[S16]
Si/MWCNT (7:3)	1770 at 50 mA/g	1250 at 50 mA/g after 50 cycles	[S17]
Si/MWCNT (5:5)	1182 at 50 mA/g	889 at 50 mA/g after 50 cycles	[S17]

[1]N-CNTs- nitrogen doped carbon nanotubes, [2]N-CNFs-nitrogen doped carbon nanofibers, [3]PGC-porous graphitic carbon, MWCNT-multiwalled carbon nanotubes

Supporting Information S8

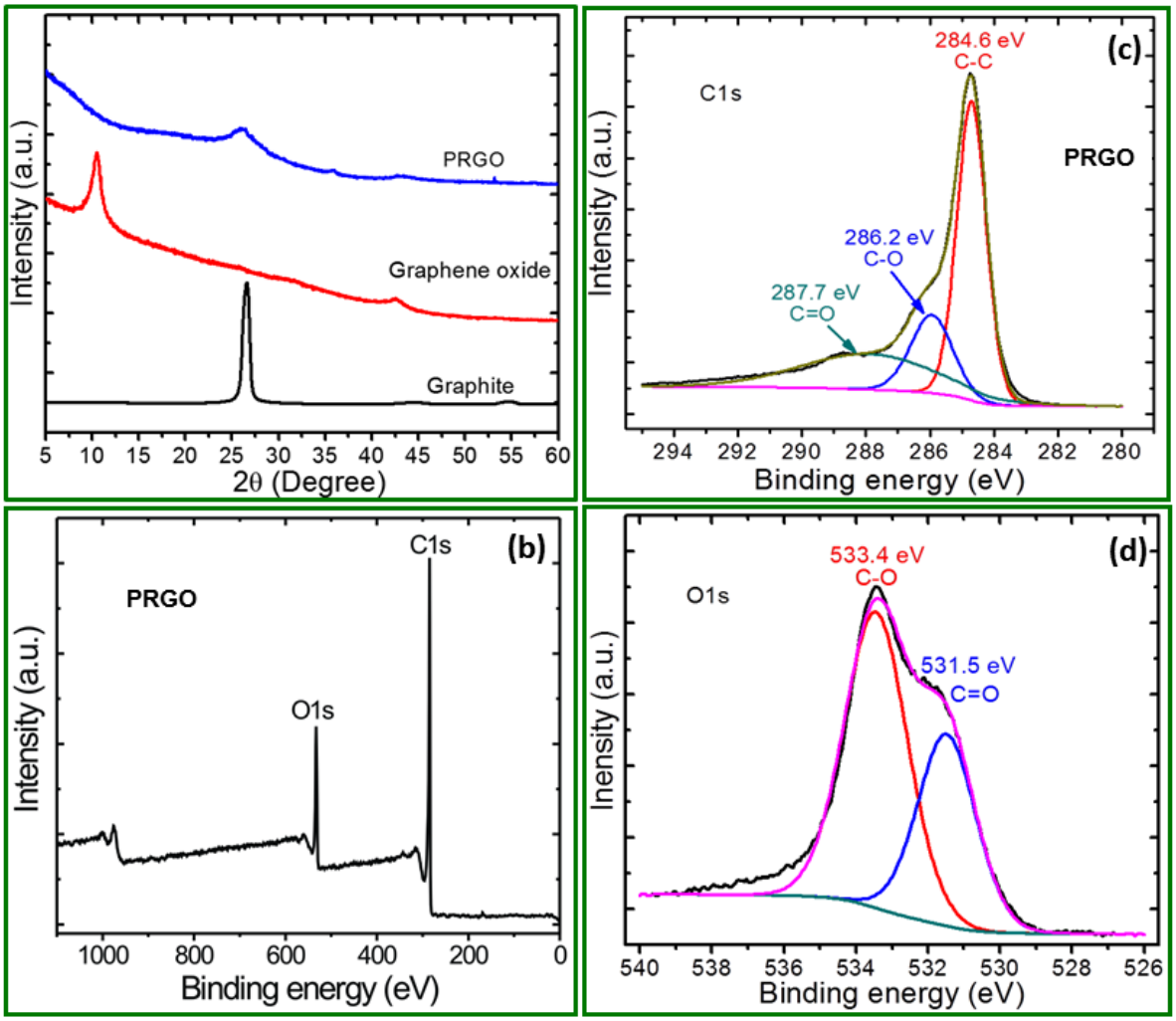

Figure S8 (a) XRD patterns of graphite, graphene oxide and partially reduced graphene oxide (PRGO), showing considerable change in the structure. (b) Full XPS spectrum of PRGO, suggesting the presence of C1s and O1s, confirming the presence of enough oxygen functional groups (~34 %) which can acts as centers for Li-ion storage in a pseudocapacitive mechanism.

Supporting Information S9

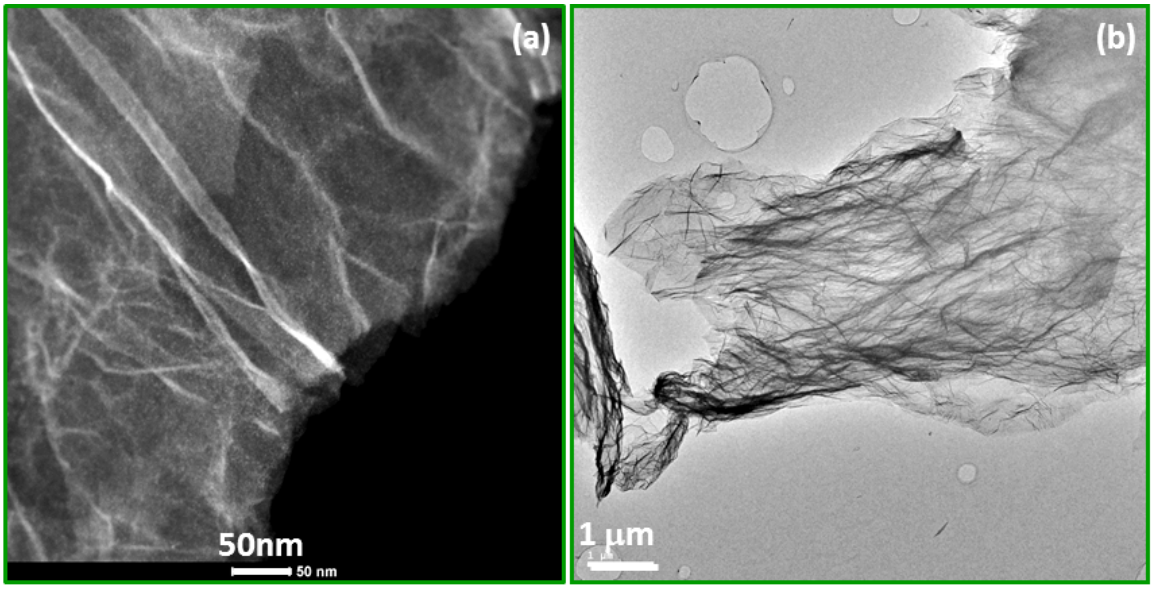

Figure S9 (a, b) EFTEM and TEM images of partially reduced graphene oxide (PRGO) suggesting, highly porous interconnected nanosheets network. Also the nanosheets are extremely thin and transparent.

Supporting Information S10

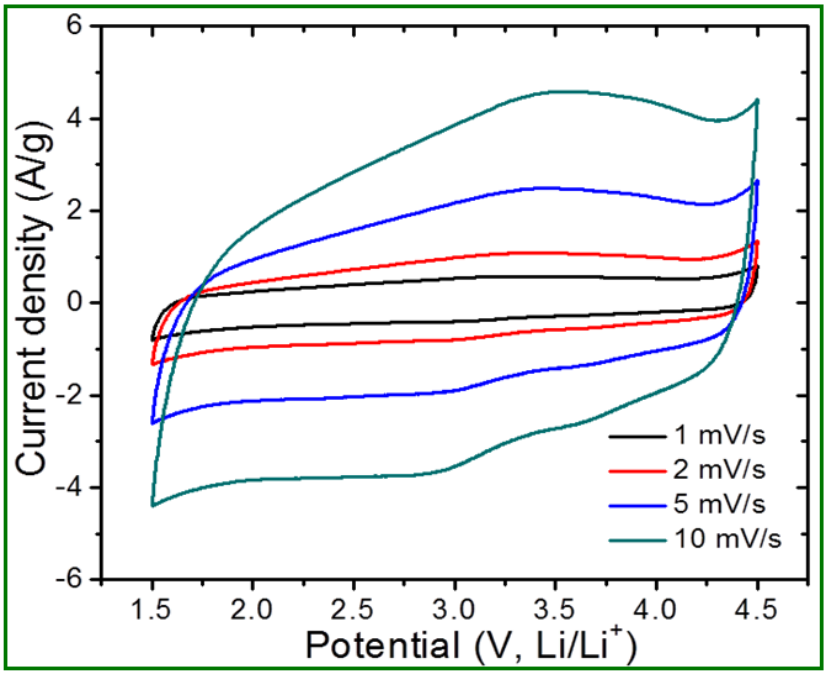

Figure S10 CV curves for partially reduced graphene oxide (PRGO) electrode in a Li half-cell within the potential range of 1.5 to 4.5 V (vs Li/Li^+) at different scan rates.

Supporting Information S11

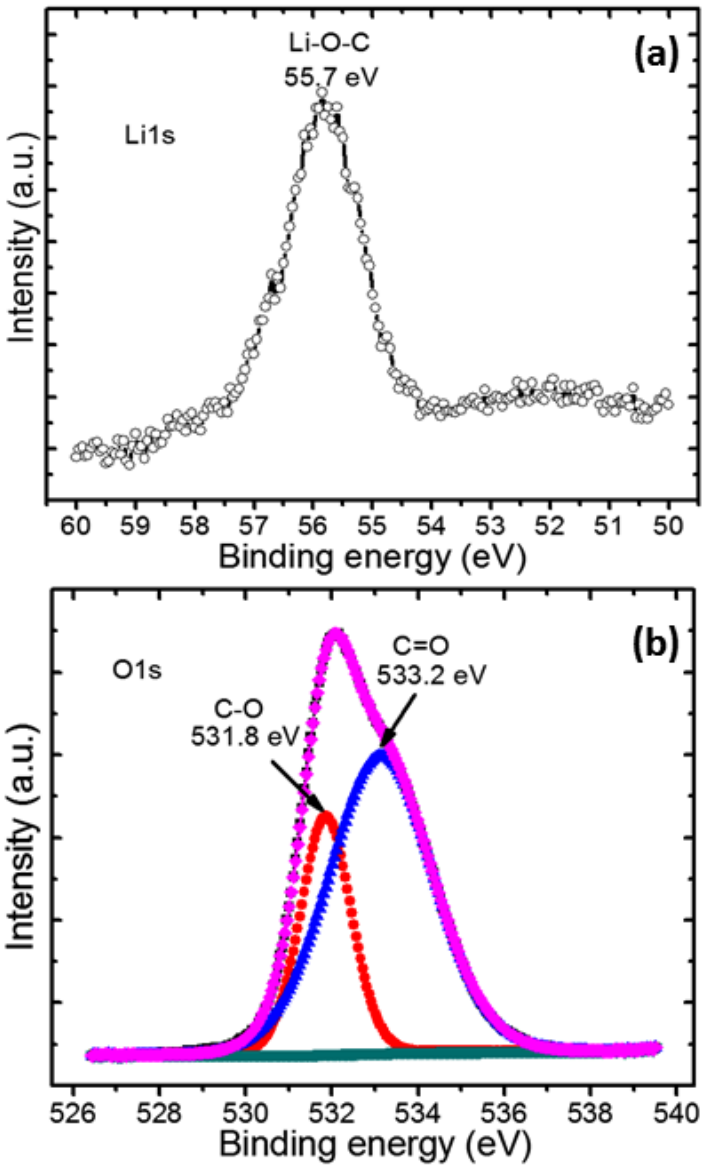

Figure S11 (a, b) High magnified XPS spectra of Li1s and O1s of for PRGO electrode after 2000 cycles in half cell configuration, respectively. Functional groups such as C=O and C-O are detected, which are responsible for Li storage in a pseudocapacitive mechanism.

Supporting Information S12

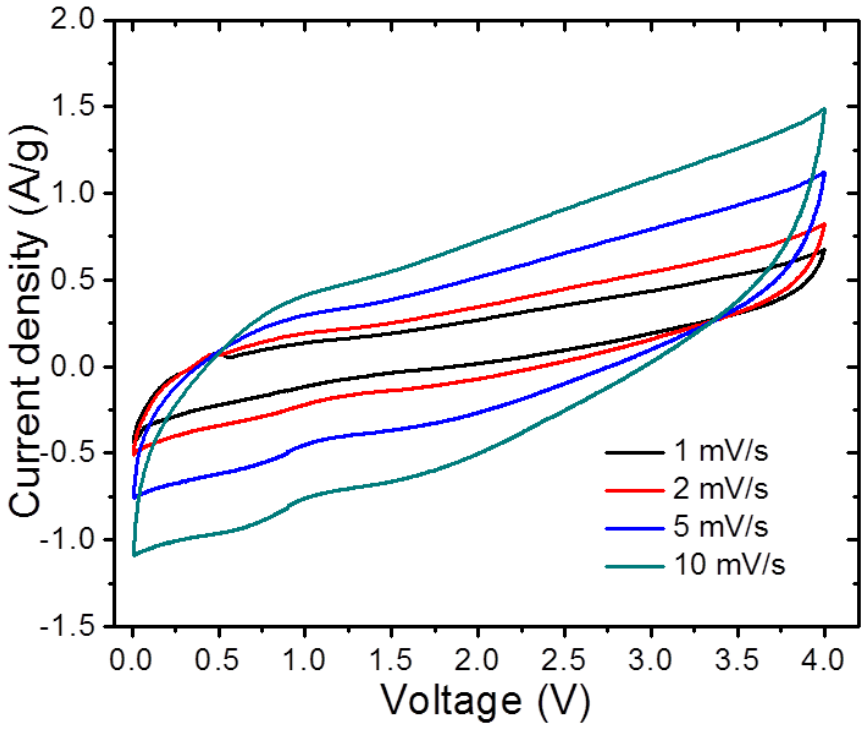

Figure S12 CV curves for N-CNPipes//PRGO Li-ion capacitor full cell within high working voltage range from 0.0 to 4.0 V.

Supporting Information S13

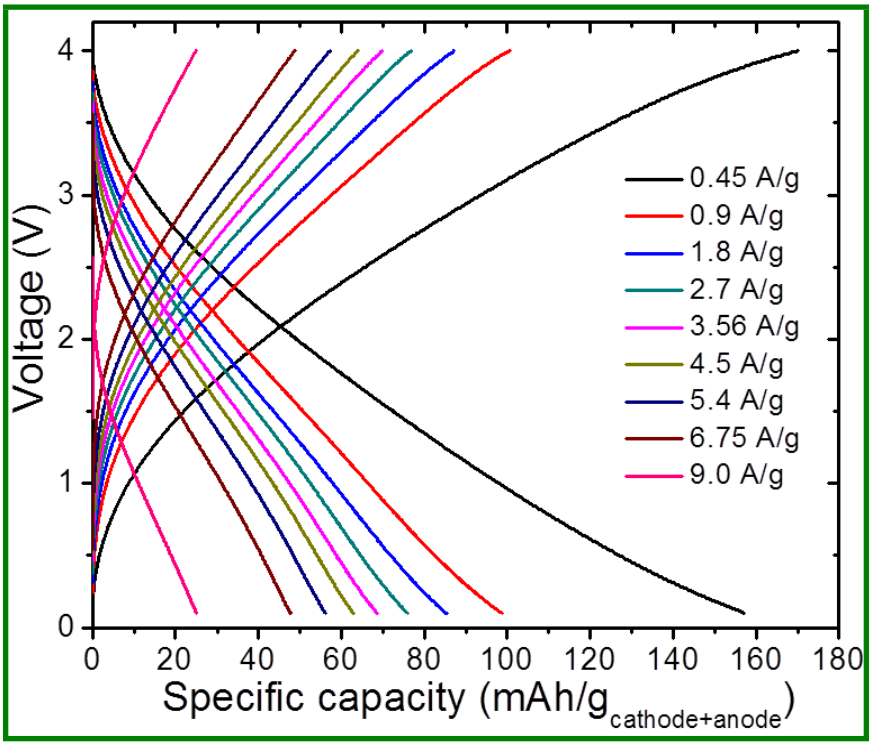

Figure S13 Plot of specific capacity considering mass of active materials in both cathode and anode with current density in Li organic electrolyte between 0 to 4 V suggesting almost 100% utilization of cathode material.

Supporting Information S14

The discharge capacitance (C_{cell}) of the N-CNPipes//PRGO LIC was derived as

$$C_{cell} = (it/m\Delta V) \qquad (1)$$

where i is the applied current, ΔV is the potential difference, t is the discharge time and m is the total mass of the two electrodes.

The power (P) and energy (E) densities were calculated from the following equations,

$$P = \frac{\Delta V \times i}{m} \qquad (2)$$

$$E = \frac{P \times t}{3600} \qquad (3)$$

$$\Delta V = \frac{(E_{\max} + E_{\min})}{2} \qquad (4)$$

where, E_{max} and E_{min} are the voltages at the beginning and end of the discharge, 't' is the discharge time, 'I' is the discharge current, and 'm' is the total mass of active materials in the anode and cathode (1.9 to 2 mg).

Supporting Information Table 2

Table 2 Comparison of published electrochemical properties of Li-ion capacitors with our present work

LIC cell	Energy density (Wh/kg)	Power density (W/kg)	Voltage (V)	Cycling stability	References
N-CNPipes//PRGO	262 at 450 W/kg	9000 at 78 Wh/kg	4.0	89 % after 1000 cycles	Present work
rGO//FGO[1]	225 at 110 W/kg	6450 at 70 Wh/kg	4.1	54 % after 2000 cycles	[S18]
$Li_4Ti_5O_{12}$//AC[2]	67.5 at 490 W/kg	4995 at 33.6 Wh/kg	3.0	85 % after 2000 cycles	[S19]
Graphene//FRGO[3]	148.3 at 141 W/kg	7800 at 71.5 Wh/kg	4.2	68 % after 3000 cycles	[S20]
Graphene-$Li_4Ti_5O_{12}$// Graphene/Sucrose	95 at 40 W/kg	3000 at 32 Wh/kg	3.0	87 % after 500 cycles	[S21]
Li_3VO_4//AC	49.1 at 72.5 W/kg	24.5 at 129.7 Wh/kg	3.5	-	[S22]
$LiTi_{1.5}Zr_{0.5}(PO_4)_3$// AC	46.7 at 79.2 W/kg	8120 at 9.91 Wh/kg	3.4	93 % after 100 cycles	[S23]
Fe_3O_4-Graphene// 3D Graphene	147 at 150 W/kg	2587 at 86 Wh/kg	3.0	70 % after 1000 cycles	[S24]
TiC//PHPNC[4]	112 at 450 W/kg	67500 at 35.6 Wh/kg	4.5	83%, 5000 cycles	[S25]
Graphene-VN //carbon nanorods	162 at 200 W/kg	10000 at 64 Wh/kg	4.0	86%, 1000 cycles	[S26]
CNT/V_2O_5//AC	25.5 at 40 W/kg	6300 at 6.9 Wh/kg	2.7	80%, 10000 cycles	[S27]

TiO_2-B nanowire//CNT	12.5 at 300 W/kg	1300 at 8 Wh/kg	2.8	1000 cycles	[S28]
TiP_2O_7//AC	13 at 46 W/kg	370 at 0.2 Wh/kg	3.0	78%, 500 cycles	[S29]
Li-Hard carbon//AC	82 at 100 W/kg	50000 at 1 Wh/kg	2.8	100 % after 40 cycles	[S30]

[1]FGO-functionalized graphene oxide, [2]AC-activated carbon, [3]FRGO-flash reduced graphene oxide, [4]PHPNC- pyridine-derived hierarchical porous nitrogen-doped carbon

Supporting Information S15

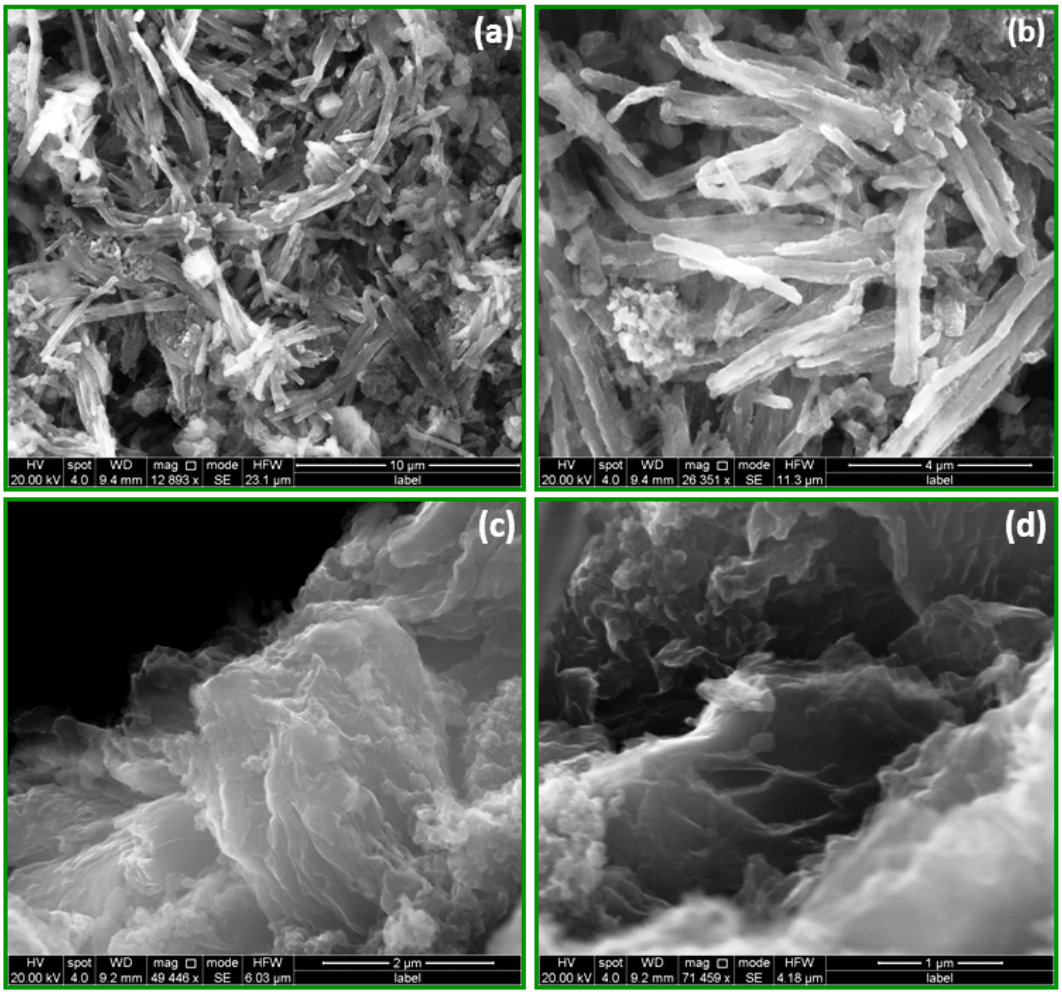

Figure S15 FESEM images of (a, b) N-CNPipes and (c, d) PRGO after 1000 charge/discharge cycles at two different magnifications.

References

[S1] Dubal, D. P.; et al. Synthetic approach from polypyrrole nanotubes to nitrogen doped pyrolyzed carbon nanotubes for asymmetric supercapacitors, *J. Power Sources* **308**, 158-165 (2016).

[S2] Li, X. *et. al.* High concentration nitrogen doped carbon nanotube anodes with superior Li+ storage performance for lithium rechargeable battery application, *J. Power Sources* **197**, 238-245 (2012).

[S3] Qie, L. et al. Nitrogen-doped porous carbon nanofiber webs as anodes for lithium ion batteries with a superhigh capacity and rate capability,*Adv.Mater.***24**, 2047-2050 (2012).

[S4] Bulusheva, L. G. et al. Electrochemical properties of nitrogen-doped carbon nanotube anode in Li-ion batteries, *Carbon*, **49**, 4013-4023 (2011).

[S5] Reddy, A. L. M. et al., Synthesis of nitrogen-doped graphene films for lithium battery application, *ACS Nano*, **4**, 6337-6342 (2010)

[S6] Shin, W. H., Jeong, H. M., Kim, B. G., Kang, J. K., Choi, J. W., Nitrogen-doped multiwall carbon nanotubes for lithium storage with extremely high capacity, *Nano Lett.* **12**, 2283-2288 (2012).

[S7] Lim, J., Li, D., Kwon, J. Kim, S. O., Open-ended N-doped carbon nanotubes array for Li-ion battery anode, *Proceedings of the World Congress on New Technologies*, Barcelona, Spain- July 15-17, 2015 Paper No. 460

[S8] Lee, S. W. et al., High-power lithium batteries from functionalized carbon-nanotube electrodes, *Nat. Nanotech.* **5**, 531-537 (2010)

[S9] Chen, Y. et al., Hollow carbon-nanotube/carbon-nanofiber hybrid anodes for Li-Ion batteries, *J. Am. Chem. Soc.*, **135**, 16280-16283 (2013)

[S10] Chen, L. et al., Porous graphitic carbon nanosheets as a high-rate anode material for lithium-ion batteries, *ACS Appl. Mater. Interfaces*, **5**, 9537–9545 (2013)

[S11] Zhang, W. M., Wu, X. L., Hu, J. S., Guo, Y. G., Wan, L. J., Carbon coated Fe_3O_4 nanospindles as a superior anode material for lithium-ion batteries, *Adv. Funct. Mater.* **18**, 3941-3946 (2008)

[S12] Wu, Z. S., Ren, W., Xu, L., Li, F., Cheng, H. M., Doped graphene sheets as anode materials with superhigh rate and large capacity for lithium ion batteries, *ACS Nano*, **5**, 5463-5471 (2011)

[S13] Zhou, G.et al., Graphene-wrapped Fe_3O_4 anode material with improved reversible capacity and cyclic stability for lithium ion batteries, *Chem.Mater.* **22**, 5306-5313 (2010)

[S14] Chen, W. X., Lee, J. Y., Liu, Z. L., The nanocomposites of carbon nanotube with Sb and $SnSb_{0.5}$ as Li-ion battery anodes. *Carbon* **41**, 959-966 (2003)

[S15] Huang, H., Zhang, W. K., Gan, X. P., Wang, C., Zhang, L., Electrochemical investigation of TiO_2/carbon nanotubes nanocomposite as anode materials for lithium-ion batteries, *Mater. Lett.* **61**, 296-299 (2007)

[S16] Fu, Y., Ma, R., Shu, Y., Cao, Z., Ma, X., Preparation and characterization of SnO_2/carbon nanotube composite for lithium ion battery applications, *Mater. Lett.* **63**, 1946-1948 (2009).

[S17] Wen, Z., Wang, Q., Zhang, Q., Li, J., In situ growth of mesoporous SnO_2 on multiwalled carbon nanotubes: a novel composite with porous-tube structure as anode for lithium batteries, *Adv. Funct. Mater*. **17**, 2772-2778 (2007)

[S18] Kim, H.; Park, K. Y.; Hong, J.; Kang, K.; All-graphene-battery: bridging the gap between supercapacitors and lithium ion batteries, *Sci. Rep.* **4**, 5278 (2014)

[S19] Jain, A. et al., Activated carbons derived from coconut shells as high energy density cathode material for Li-ion capacitors, *Sci. Rep.* **3**, 3002 (2013)

[S20] Zhang, T. et al., High energy density Li-ion capacitor assembled with all graphene-based electrodes, *Carbon* **92**, 106-118 (2015).

[S21] Leng, K. et al., Graphene-based Li-ion hybrid supercapacitors with ultrahigh performance, *Nano Res.* **6**, 581-592 (2013).

[S22] Wei, H. Y., Tsai, D. S., Hsieh, C. L., Prelithiated lithium vanadate anode and the mass balancing of its hybrid capacitor, *RSC Adv.*, **5**, 69176-69183 (2015)

[S23] Peng, C. J., Tsai, D. S., Chang, C., Wei, H. Y., The lithium ion capacitor with a negative electrode of lithium titanium zirconium phosphate, *J. Power Sources* **274**, 15-21 (2015)

[S24] Zhang, F. et al., A high-performance supercapacitor-battery hybrid energy storage device based on graphene-enhanced electrode materials with ultrahigh energy density, *Energy Environ. Sci.*, **6**, 1623-1632 (2013)

[S25] Wang, H.; et al. A high-energy lithium-ion capacitor by integration of a 3D interconnected titanium carbide nanoparticle chain anode with a pyridine-derived porous nitrogen-doped carbon cathode, *Adv. Funct. Mater.***26**, 3082-3093 (2016)

[S26] Wang, R., Lang, J., Zhang, P., Lin, Z., Yan, X., Fast and Large Lithium Storage in 3D Porous VN Nanowires–Graphene Composite as a Superior Anode Toward High-Performance Hybrid Supercapacitors, *Adv. Funct. Mater*. **25**, 2270-2278 (2015)

[S27] Chen, Z. et al., High-Performance Supercapacitors Based on Intertwined CNT/V_2O_5 Nanowire Nanocomposites, *Adv. Mater.* **23**, 791-795 (2011)

[S28] Wang, Q., Wen, Z., Li, J., A Hybrid Supercapacitor Fabricated with a Carbon Nanotube Cathode and a TiO_2–B Nanowire Anode, *Adv. Funct. Mater*. **16**, 2141-2146 (2006)

[S29] Aravindan, V. et al., Hybrid supercapacitor with nano-TiP_2O_7 as intercalation electrode, *J. Power Sources*, **196**, 8850-8854 (2011)

[S30] Cao, W. J., Zheng, J. P., Li-ion capacitors with carbon cathode and hard carbon/stabilized lithium metal powder anode electrodes, *J. Power Sources* **213**, 180-185 (2012)